A mixed source for the Late Triassic Garzê-Daocheng granitic belt and its implications for the tectonic evolution of Yidun arc belt, eastern Tibetan Plateau

Tao Wu[1,2], Long Xiao[2,3]*, Simon A. Wilde[4], Chang-Qian Ma[2,3], Jia-Xi Zhou[5]

[1]School of Earth Sciences, Zhejiang University, Hangzhou 310027, China

[2]School of Earth Science, China University of Geosciences, 388 Lumo Rd, Hongshan District, Wuhan 430074, China

[3]State Key Laboratory of Geological Processes and Mineral Resources, China University of Geosciences, 430074, Wuhan, China

[4]Department of Applied Geology, Curtin University, GPO Box U1987, Perth, Western Australia 6845, Australia

[5]School of Resource Environment and Earth Sciences, Yunnan University, Kunming 650091, China

[*]Corresponding author. Tel.: +86 27 6788 3048; fax: +86 27 67883001. E-mail address: longxiao@cug.edu.cn (L. Xiao).

Abstract: Many Late Triassic granitic plutons are present in the eastern Yidun arc belt (YAB), and seven have been investigated in this study. From west to east, they are: the Sucuoma (235 ± 2 Ma), Ajisenduo (224 ± 2 Ma), Jiaduocuo (218 ± 1 Ma),

Cuojiaoma (219 ± 1 Ma), Maxionggou (225 ± 2 Ma), Dongcuo (222 ± 3 Ma) and Daocheng (220 ± 2 Ma) plutons. Most of the plutons have granitic compositions and contain high SiO_2, Al_2O_3 and K_2O+Na_2O, but low MgO, FeO* and CaO contents. They have similar trace element patterns, with depletion in high field strength elements (HFSE, e.g., Nb, Ta and Zr) and enrichment in large-ion lithophile elements (LILE, e.g., Rb, Th and U). Samples from the Sucuoma, Jiaduocuo and Dongcuo plutons have similar zircon Hf isotopic compositions ($\varepsilon_{Hf}(t)$ = -1.8 to -0.3, -3.1 to 0.4 and -4.6 to -1.4, respectively), whereas those from the Ajisenduo pluton exhibit more unradiogenic Hf ($\varepsilon_{Hf}(t)$ = -11.9 to -4.8). Additionally, the Sucuoma pluton has the lowest initial $^{87}Sr/^{86}Sr$ values (0.7060 - 0.7090) but the least negetive $\varepsilon_{Nd}(t)$ (-4.9 to -3.3) values, whereas samples from the Ajisenduo pluton have the highest initial $^{87}Sr/^{86}Sr$ values (0.7111 - 0.7160), but the most negative $\varepsilon_{Nd}(t)$ values (-7.9 and -11.3). All the samples have similar high radiogenic Pb isotopic compositions ($^{206}Pb/^{204}Pb$ = 18.6 - 19.4; $^{207}Pb/^{204}Pb$ = 15.7 - 15.8; $^{208}Pb/^{204}Pb$ = 39.1 to 40.4). Based on the new geochemical data, it is determined that most of the granitoids are I-type granites and the magma source was a mixture of the metamorphic Kangding Complex, which is considered to be the basement of the western Yangtze Craton, and metasediments from the basement. However, the samples from the Ajisenduo pluton are S-type granites that were derived from partial melting of basement metasediments with only limited components from the Kangding Complex. Together with an evaluation of previously-published work, these new data indicate a dominant magmatic peak at ~216 Ma for the Late Triassic granitoids of the YAB and that the ages of Late Triassic magmatism become younger eastward towards the Garzê-Litang suture zone. We consider that slab roll-back, with subsequent slab break-off, best explains the origin of these granitic plutons.

Key words: Yidun Arc Belt; Sr-Nd-Hf-Pb isotopes; granites; slab roll-back; Eastern Tibetan Plateau

1. Introduction

The Sanjiang orogenic belt in southwest China (Fig.1a) is a major component of the Tethyan giant metallogenic belt (Hou et al., 2007). It lies along the eastern margin of Tibetan Plateau and contains three N-S trending Paleozoic sutures (the Changning-Menglian suture zone, Jinshajiang-Ailaoshan suture zone and Garzê-Litang suture zone) related to the breakup of Gondwanaland (Fig.1a, b; Wang et al., 2000; Xiao et al., 2008). There are also four volcanic arcs named, from west to east, the Zaduo-Jinghong continental margin arc, the Jiangda-Weixi continental margin arc, the Yaxuanqiao arc and the Yidun arc (Fig.1b). This study focuses on the Yidun arc belt (YAB), which is located in the northeastern part of the Sanjiang orogenic belt (Fig.2a). Based on the distribution of strata, the YAB can be divided into the eastern and western YAB (EYAB and WYAB, respectively). There are three subsidiary arcs located within the EYAB named, from north to south, the Changtai arc, Xiangcheng arc and Zhongdian arc, whereas the sediments of the WYAB are all older than Triassic and usually referred to as the Zhongza massif (Fig. 2c, d). It has generally been considered that the YAB formed by westward subduction of the Garzê-Litang oceanic slab in the Late Triassic (Chen et al., 1987; Hou and Mo, 1991; Hou et al., 2003). There are three main tectonic models that have been suggested for the formation of the YAB: (1) it formed by westward subduction of the Garzê-Litang oceanic slab, however, along 30° N, the subduction angle of the northern oceanic slab is much steeper than the southern segment (Hou et al., 2003, 2004); (2) the Triassic tectonomagmatic evolution of the YAB involved two stages of subduction of the Garzê-Litang Ocean (Wang et al., 2013a). Early stage subduction (~230-224 Ma) was along the southern end of the YAB, whereas the second stage was along the east; and (3) the northern YAB (Changtai arc) was an island arc, whereas the southern one (Zhongdian arc) was a continental margin arc (Leng et al., 2014).

The huge Late Triassic Garzê-Daocheng granitic belt is located in the EYAB (Fig. 2a). However, the petrogenesis and tectonic background of these granites is controversial. One group of workers has suggested that they are I-type granites, derived from partial melting of the Late Paleoproterozoic basement (e.g., Hou et al., 2001, 2003; He et al., 2013). The other group has suggested they were derived from metasediments (e.g., Liu et al., 2006). The Garzê-Daocheng granitic belt has been interpreted to have formed either in an arc setting (Wang et al., 2013a, b) or a post-orogenic extensional setting (Peng et al., 2014). A further complicating factor is that the sediments in the EYAB are Triassic in age, and no basement rocks are exposed. Some researchers have considered there is Precambrian basement of western Yangtze Craton affinity beneath the Triassic sedimentary rocks of the EYAB, and that it was a continental margin arc (e.g., He et al., 2013; Wu et al., 2016b), whereas others have proposed the southern part of the EYAB was developed on a crustal basement and the northern part on oceanic crust (e.g., Leng et al., 2014). However, most studies have focused on the southern part of the granitic belt (e.g., He et al., 2013; Peng et al., 2014) and the granites in the northern part (e.g. the Sucuoma, Jiaduocuo, Ajisenduo and Sucuoma plutons) have not been systemically studied. Their petrography and petrogenesis is unknown and this limits our understanding of the evolution of the whole of the YAB in the Late Triassic.

In recent years, many Triassic granitic plutons have been recognized in the EYAB, including, from west to east, the Sucuoma (SCM), Ajisenduom (ZK), Jiaduocuo (JDC), Cuojiaoma (CJM), Maxionggou (MXG), Dongcuo (HZS) and Daocheng (DC) plutons (Fig. 2a), which provide a good opportunity to further constrain the evolutionary history of the YAB in the Late Triassic, as well as the nature of the basement to the EYAB. In this contribution, we present zircon U-Pb geochronology, whole-rock major and trace element data, and Sr-Nd-Hf-Pb isotopes of these plutons in order to determine their formation ages, petrogenesis and tectonic setting.

2. Geological background

The Garzê-Litang suture zone defines the boundary between the Songpan-Garzê terrane to the east and the Yidun Arc belt (YAB) to the west (Fig. 2a). It is 5 - 20 km wide and over 500 km long, extending from southeastern Qinghai Province to western Yunnan Province. It contains metamorphosed peridotite, dolerite dikes, and pillow lavas (Hou et al., 2004). The Garzê-Litang ocean opened in the Late Permian, as a result of either a plume beneath the western margin of the Yangtze Craton (e.g., Chen et al., 1987; Song et al., 2004; Xiao et al., 2008) or eastward subduction of the Jinshajiang ocean along the Jinshajiang suture (e.g., Roger et al., 2008, 2010; Zhang and Jin, 1979). However, some authors also have considered that the Garzê-Litang ocean was opened in the early Permian (292Ma; Yan et al., 2005). The Garzê-Litang ocean began to subduct westward to form the YAB during the Late Triassic (Chen et al., 1987; Hou et al., 2001, 2004).

The WYAB, also known as the Zhongza massif (Fig. 2a), is dominated by weakly metamorphosed Paleozoic carbonate, clastic rocks and minor mafic volcanic rocks with a Neoproterozoic basement composed of granitic gneisses and meta-volcanic rocks (BGMRSP, 1991; Liu et al., 1996). It has been proposed that the Zhongza massif rifted from the western Yangtze Craton during the opening of the Garzê-Litang ocean in the late Palaeozoic, based on their stratigraphic similarity, which includes basalts geochemically similar to the Emeishan basalts (Mo et al., 1993; Pan et al., 1997; Hou et al., 2003).

The EYAB, which is dominated by Triassic volcano-sedimentary successions, can be further divided into the NYAB and SYAB based on the differences in rock assemblages and mineralization (Fig. 2c). In the NYAB (the Changtai arc), widespread Late Triassic bimodal volcanic suites and arc-type volcanic rocks host multiple sulfide deposits (Hou et al., 2003). However, the SYAB (the Zhongdian arc), is characterized by calc-alkaline andesitic-dacitic volcanic rocks and associated porphyry complexes and contains several porphyry-type or skarn-type Cu-polymetallic deposits (Hou et al., 2007). Triassic granitic plutons in the YAB are mainly subduction/arc-related, calc-alkaline, I-type granites that formed between 237 Ma and 206 Ma (Hou et al., 2001; Reid et al., 2007; Wang et al., 2011) and are distributed along a N-S trending belt that is parallel to the Garzê-Litang suture zone (Fig. 2a). Although Jurassic and Cretaceous sediments are absent in the YAB, a belt of Cretaceous granites does occur in the central part. Most of the Cretaceous granites are A-types and formed between 107 Ma and 77 Ma (Hou et al., 2001; Qu et al., 2002; Reid et al., 2007; Wu et al., 2014a). A Late Jurassic mafic intrusion has also been reported from the area (Wu et al., 2014b).

3. Samples and Petrography

Thirty-seven samples (N=37) were collected from plutons in the EYAB: Sucuoma (N=9), Ajisenduom (N=4), Jiaduocuo (N=4), Cuojiaoma (N=6), Maxionggou (N=3), Dongcuo (N=7) and Daocheng (N=4) (Fig. 2a).

The Sucuoma pluton intruded the Upper Triassic Qugasi Fomation (T_3q) and crops out over ~80 km^2. The rock types are granodiorite and monzogranite, with some porphyritic monzogranite. The granodiorite is fine- to medium-grained (1-3 mm) and consists of quartz (~20 vol.%), plagioclase (40 - 50 vol.%), potassium feldspar (10 - 20 vol.%), biotite and amphibole (totalling 5 - 10 vol.%) (Fig. 3b). The porphyritic monzogranite contains phenocrysts of perthite, with minor quartz and plagioclase (10 - 30 vol.%) (Fig. 3c,d). The groundmass is composed of perthite (30

- 45 vol.%), plagioclase (20 - 30 vol.%), quartz (~20 vol.%) and biotite (~5 vol.%). The monzogranite is medium- to coarse-grained and composed of quartz (20 - 25 vol.%), plagioclase (30 - 40 vol.%), potassium feldspar (30 - 40 vol.%), biotite and amphibole (totalling 5 - 10 vol.%) (Fig. 3e).

The other plutons also consist of granodiorite, monzogranite, and porphyritic monzogranite. The granodiorites are composed of quartz (~20 vol.%), plagioclase (50 - 60 vol.%), potassium feldspar (10 - 20 vol.%), biotite and amphibole (totaling 5 - 10 vol.%) (Fig. 3g). The monzogranites contain quartz (20 - 30 vol.%), plagioclase (25 - 30 vol.%), potassium feldspar (35 - 45 vol.%) and biotite (~5 vol.%). Samples from Ajisenduo pluton also have muscovite (Fig. 3f). The porphyritic monzogranite has phenocrysts (10 - 20 vol.%) mainly composed of perthite, with minor quartz and plagioclase. The groundmass comprises quartz (20 - 35 vol.%), plagioclase (25 - 35 vol.%), potassium feldspar (20 - 30 vol.%), biotite and amphibole (totalling 5 - 10 vol.%) (Fig. 3h).

4. Analytical methods

Zircon grains were separated using conventional heavy liquid and magnetic techniques, handpicked, and then mounted in epoxy and polished. After the samples were carbon coated, cathodoluminescence images were taken to select sites for analysis. U-Pb dating and trace element analyses were conducted synchronously by LA-ICP-MS at the State Key Laboratory of Geological Processes and Mineral Resources (GPMR), China University of Geosciences, Wuhan. Detailed operating conditions for the laser ablation system, the ICP-MS and data reduction were the same as those outlined by Liu et al. (2010).

In situ zircon Hf isotopic analyses were undertaken on a Neptune Plus MC-ICP-MS (Thermo Fisher Scientific, Germany) in combination with a Geolas 2005 excimer ArF laser ablation system (Lambda Physik, Göttingen, Germany) hosted at the GPMR. We selected the same CL domains for analysis. Zircon 91500, GJ-1 and TEM were used as the standards and the analytical values of $^{176}Hf/^{177}Hf$ are 0.282294-0.282320, 0.282008-0.282030, and 0.282672-0.282086, respectively. Detailed operating conditions for the laser ablation system, MC-ICP-MS and analytical methods were the same as outlined by Hu et al. (2012).

Whole-rock major elements analyses were determined by X-ray fluorescence spectrometry (XRF) at the Hubei Geological Research Laboratory (HGRL). Accuracy and precision of the XRF analyses are estimated to be 5%. Trace element analyses were conducted by LA-ICP-MS at the GPMR. Accuracy and precision of the LA-ICP-MS analyses are estimated to be less than 10%. Detailed operating conditions for the laser ablation system, ICP-MS and data reduction were the same as Liu et al. (2008).

Whole rock Sr-Nd-Pb isotopic compositions were analyzed at the Guangzhou Institute of Geochemistry, Chinese Academy of Sciences (GIGCAS). Whole rock Sr - Nd isotope data were obtained using a Micromass Isoprobe MC-ICP-MS. Total procedural Sr and Nd blanks were <4 ng and <1 ng, respectively. Details of the methods are given in Wei et al. (2002) and Li et al. (2004). For Pb isotope analyses, the weighed samples were dissolved in Teflon capsules with purified HF at 120℃ for two days. $HClO_4$ was added to the capsules and the solution was desiccated. Lead was separated by anion-exchange columns with diluted HBr as eluant. The isotopic analyses were performed using a Micromass Isoprobe Multi-Collector ICPMS at GIG-CAS.

5 Results

5.1 Geochronology

Eight granitic samples from the plutons were selected for zircon U-Pb dating. They were collected from the Sucuoma (SCM-10), Ajisenduo (ZK-1), Jiaduocuo (JDC-2), Cuojiaoma (CJM-6), Dongcuo (HZS-8 and HZS-14), Daocheng (DC-9) and Maxionggou (MXG-1) plutons (Fig. 2a). Most of the zircons are pale pink to colorless prismatic crystals and 100 - 200 μm in size. Euhedral oscillatory zoning is common in most crystals. Th/U ratios range from 0.2 to 1, indicating a magmatic origin. The results are listed in Table S1 and U-Pb concordia diagrams and representative zircon CL images are shown in Fig. 4.

Nineteen zircon crystals from sample SCM-10 from the Sucuoma plution were dated and eighteen sites record $^{206}Pb/^{238}U$ ages ranging from 230 Ma to 241 Ma, and define a weighted mean age of 235 ± 2 Ma (N=18, MSWD=2.1) (Fig. 4a, b), which is interpreted as the crystallization age of the granite. One slightly discordant zircon yields an apparent age of 593 Ma and is interpreted as an inherited zircon.

Nineteen sites were analyzed from sample ZK-1 from the Ajisenduo pluton.

Fourteen of them yielded $^{206}Pb/^{238}U$ ages ranging from 221 to 229 Ma with a weighted mean age of 224±2 Ma (N=14, MSWD=1.2) (Fig. 4c, d), which is considered to be the crystallization age of the granite. The other five grains yielded concordant ages ranging from 330 to 1573 Ma and are interpreted as inherited zircons.

For sample JDC-2 from the Jiaduocuo pluton, nineteen zircons were analyzed. Except for one older grain (339 Ma) (Fig. 4e) the other eighteen grains yielded $^{206}Pb/^{238}U$ ages ranging from 212 to 221 Ma with a weighed mean age of 218±1 Ma (N=18, MSWD=0.88). This age represents the crystallization age of the Jiaduocuo granite (Fig. 4f).

Sixteen zircon crystals from sample CJM-6 from the Cuojiaoma pluton were analyzed by LA-ICP-MS. Fifteen of them gave ages ranging from 216 Ma to 224 Ma. They plot on or near concordia with a weighted mean $^{206}Pb/^{238}U$ age of 219±1 Ma (N=15, MSWD=1.2). One older discordant analysis (657±23 Ma) is interpreted as an inherited zircon (Fig. 4g, h).

Two granitic samples (HZS-8 and HZS-14) from the Dongcuo pluton were selected for U-Pb zircon dating. Twelve analyses from sample HZS-8 have $^{206}Pb/^{238}U$ ages ranging from 217 Ma to 225 Ma and yield a weighted mean age of 222±2 Ma (N=12, MSWD=0.63) (Fig. 4i, j). One older discordant grain (1829 Ma) is interpreted as an inherited zircon. Nine analyses from sample HZS-14 yield $^{206}Pb/^{238}U$ ages of 216 Ma to 227 Ma (Fig. 4k, e) with a weighted mean age of 222±3 Ma (N=9, MSWD=2). The older discordant grains (341-2070 Ma) are interpreted as inherited zircons. The weighted mean ages of the two samples are identical and interpreted as the crystallization age of the Dongcuo pluton.

Sixteen zircons from granitic sample DC-9 from Daocheng pluton were analyzed by LA-ICP-MS. They have $^{206}Pb/^{238}U$ ages ranging from 213 Ma to 225 Ma, yielding a weighted mean age of 220±2 Ma (N=16, MSWD=2.3), which is interpreted as the crystallization age of the granite.

Sixteen zircons from granitic sample MXG-1 from the Maxionggou pluton were analyzed, with $^{206}Pb/^{238}U$ ages ranging from 222 Ma to 229 Ma, with a weighted mean age of 225±2 Ma (N=16, MSWD=2.1) (Fig. 4e, f). This age is considered as the formation age of this pluton.

5.2 Zircon Hf isotopes

In order to investigate the change in zircon Lu-Hf isotope compositions from the inner YAB to the Garzê-Litang suture zone, we chose four represent samples (SCM-10, ZK-1, JDC-2 and HZS-8), extending from west to the east across the study area. Analyses were undertaken on the same CL zircon domains investigated for U-Pb age, and the results are listed in Table S2. The $^{176}Lu/^{177}Hf$ values are low (0.00077 - 0.00131 for SCM-10, 0.00102 - 0.00322 for ZK-1, 0.00105 - 0.00244 for JDC-2, and 0.00082 - 0.00164 for HZS-8, respectively). Zircons from samples SCM-10, JDC-2 and HZS-8 record similar $^{176}Hf/^{177}Hf$ ratios (0.28259 - 0.28263, 0.28255 - 0.28265 and 0.28241 - 0.28260, respectively) and $\varepsilon_{Hf}(t)$ values (-1.6 to -0.1, -3.2 to 0.2 and -8.2 to -1.4, respectively), whereas zircons from sample ZK-1 exhibit lower $^{176}Hf/^{177}Hf$ ratios (0.28230 - 0.28250) and more enriched $\varepsilon_{Hf}(t)$ values (-11.9 to -4.8) (Fig. 5). The latter also record older T_{DM2} model ages (1.6 - 2.0 Ga) than the other three samples (1.2 -1.8 Ga).

5.3 Sr-Nd-Pb isotopes

Seventeen samples were chosen from the Sucuoma (N=3), Ajisenduo (N=3), Jiaduocuo (N=2), Cuojiaoma (N=3) and Dongcuo (N=4) plutons for whole rock Sr-Nd isotope analysis, and nine samples were chosen from the Sucuoma (N=3), Ajisenduo (N=1), Jiaduocuo (N=2) and Cuojiaoma (N=3) plutons for whole-rock Pb-Pb analyses. The results are listed in Tables 1 and 2. Initial $^{87}Sr/^{86}Sr$ values and Nd isotopic data $\varepsilon_{Nd}(t)$ were calculated at their individual formation ages. The samples from the Sucuoma pluton record the lowest initial $^{87}Sr/^{86}Sr$ values (0.7060 - 0.7082) but the least negative $\varepsilon_{Nd}(t)$ values (-4.8 to -3.2), whereas those from the Ajisenduo pluton exhibit the highest initial $^{87}Sr/^{86}Sr$ values (0.7111 - 0.7161) but most negative $\varepsilon_{Nd}(t)$ values (-7.9 and -11.3). The samples from the Jiaduocuo, Cuojiaoma and Dongcuo plutons show similar initial $^{87}Sr/^{86}Sr$ values (0.7080 - 0.7095) and negative $\varepsilon_{Nd}(t)$ values (-9.5 to -6.2).

All the nine analyzed samples have high radiogenic Pb isotopic compositions, with the present-day whole-rock Pb isotopic ratios varying from 18.6 to 19.4 for $^{206}Pb/^{204}Pb$, from 15.7 to 15.8 for $^{207}Pb/^{204}Pb$, and from 39.1 to 40.4 for $^{208}Pb/^{204}Pb$. The initial Pb isotopic ratios were calculated at the formation age of each sample by using the single-stage Pb isotopic evolution model (Zartman and Doe, 1981). The calculated initial Pb isotope ratios range from 18.4 to 18.7 for $(^{206}Pb/^{204}Pb)_t$, from 15.7 to 15.8 for $(^{207}Pb/^{204}Pb)_t$, and from 38.3 to 39.0 for $(^{208}Pb/^{204}Pb)_t$. Except one sample from the Jiaduocuo, which has lower $(^{208}Pb/^{204}Pb)_t$ value (38.3), other samples from Sucuoma, Ajisenduo, Jiaduocuo and Cuojiama have similar whole-rock Pb isotopes and no variations have been observed been them.

5.4 Whole-rock geochemistry

Major and trace element values for the complete set of Thirty-seven samples are listed in Table S3. The rocks from the Sucuoma pluton exhibit a wider range of SiO_2 (60.6 - 74.5 wt.%), Mg# (27-64), Fe_2O_{3t} (1.64 - 5.79 wt.%), CaO (1.18 - 5.78 wt.%) and K_2O+Na_2O (5.31 - 8.43 wt.%) contents than the other plutons. In Fig. 6, all samples show a strong negative correlation between MgO, CaO, Fe_2O_3*, P_2O_5 and SiO_2, and a positive correlation between K_2O, and SiO_2. All the samples are high-K, calc-alkaline, metalumious or peraluminous rocks (molar $Al_2O_3/(CaO+Na_2O+K_2O)$: 0.88-1.13) (Fig. 7a) with several samples from Sucuoma plutons are Metaluminous, whereas others are Pealuminous.

In the primitive mantle-normalized spidergrams (Fig. 8a,c,e,g,i,k,m), all the samples show similar trace element patterns, with depletion in high field strength elements (HFSE, e.g. Nb, Ta and Zr) and enrichment in large-ion lithophile elements (LILE, e.g. Rb, Th and U). Furthermore, most of samples from the Sucuoma pluton show weak or negligible Eu anomalies with slightly positive Sr anomalies, whereas the more felsic samples display strong negative Ba, Sr and Eu anomalies (Fig. 8a, b).

The samples from the Ajisenduo, Jiaduocuo, Cuojiaoma, Dongcuo, Daocheng and Maxionggou plutons have similar chondrite-normalized REE profiles, with weak negative Eu anomalies, and Eu/Eu* of 0.13 to 0.4. They also have similar $(La/Yb)_N$ ratios (3.2 -17.4) (Table S3).

6. Discussion

6.1 Fractional crystallization

The systematic decrease in MgO, Fe_2O_3 (total Fe), Al_2O_3, CaO, TiO_2 and P_2O_5 with increasing SiO_2 contents for all the samples (Fig. 6), indicating fractionation involving mafic minerals (i.e., amphibole, clinopyroxene), Fe-Ti oxides, feldspars and apatite. The depletion in Nb and Ta is considered to be related to fractionation of a Ti-bearing phase (rutile, ilmenite, titanite). In addition, the Sr and Eu negative anomalies indicate the fractional crystallization of plagioclase or else it was left behind in the source. A sharp increase in K_2O and Rb contents in samples of porphyritic monzogranite for Sucuoma pluton occurs. This has resulted in the crystallization of biotite and K-feldspar based on petrographic observation.

6.2 Petrogenetic type: S-type, I-type, or A-type?

Granites can be commonly divided into I, S and A-type, the geochemistry of them are well known (e.g., Chappell and White, 1992; Whalen et al., 1987). The presence amphibole, cordierite, and alkaline minerals are important indicators that may be used to distinguish between I-, S- and A-type granites, respectively. Most of the samples from this study plot in the unfractionated M-, I- and S-type granite (OGT) field (Fig. 7b), with the exception of one sample each from the Ajisenduo and Dongcuo plutons. Except for samples from the Ajisenduo pluton, amphibole is common in samples with A/CNK＜1.1 (Figs. 3 and 7a). They also contain low P_2O_5 that negatively correlates with Rb and show increase in Th with increasing Rb, typical of I-type granites (Fig. 7c, d; Chappell and White, 1992), whereas the Ajisenduo pluton (A/CNK > 1.1) follows the S-type granite evolutionary trend with the presence of muscovite (Fig 7c, d; 3f). Thus, the Sucuoma, Jiaduocuo, Cuojiaoma Dongcuo, Daocheng and Maxionggou granites are I-types, whereas the Ajisenduo granite is S-type.

6.3 Magma source

6.3.1 I-type granites

I-type granites are considered to be derived from partial melting of metaigneous/infracrustal rocks (Chappell and White, 1992). As shown in Fig. 9, many samples from the Sucuoma, Jiaduocuo, Cuojiaoma, Dongcuo, Daocheng and Maxionggou plutons plot in the field of basaltic source rocks. However, some samples also plot in the metagreywacke field, indicating that sediments may play a role in their genesis.

Based on previous work, especially the new U-Pb zircon ages that have been reported in recent years, and their own study, Wang and co-authors (2013a) suggested that the arc volcanic rocks formed at about 4-6 Ma earlier than the emplacement of the granitic plutons of Garzê-Daocheng belt, and hence they may derived from partial melting of the juvenile arc crust. However, the old T_{DM2} model ages of both Hf and Nd isotopes preclude a simple young arc source. Previous works have indicated that the YAB has the same basement as the western Yangtze Craton, i.e. the Kangding Complex (e.g., He et al., 2013; Wu et al., 2016a, b). In the Fig. 10a, the Sr-Nd isotopic compositons of samples from the Sucuoma pluton plot into the same field as metabasaltic rocks of the Kangding Complex, which is commonly considered as the basement of western Yangtze craton (Zhou et al., 2002). However, the samples from the other plutons plot below the field of both arc volcanic rocks and the Kangding Complex (Fig. 10a) and their zircon Lu-Hf isotopes are also more enriched than those of the Kangding Complex. Furthermore, isotopic compositions, including their whole-rock Nd and Pb isotopes, are much different for granites from the adjacent Songpan-Garzê terrane (Fig. 11a,b,c), which were also considered to have formed by partial melting of the Kangding Complex (Zhang et al., 2006; Xiao et al., 2007). This may indicate that the source of these granites was different from the Kangding Complex. The granites of the EYAB have relatively higher $^{207}Pb/^{204}Pb$ and $^{208}Pb/^{204}Pb$ values and show greater enrichment in Nd isotopes than granites in the neighbouring Songpan-Garzê terrane, implying more evolved materials were incorporated into the source region, such as metasedimentary rocks from the basement. Pre-Permian metasediments in the region are mainly distributed in the WYAB (Zhongza massif) and the major provenance of the widespread Late Triassic sediments in the EYAB was proposed to be from the Zhongza massif (Wang et al., 2013b; Wu et al., 2016b), which indicates that they could represent the composition of the pre-Permain metasediments of the WYAB. However, only Nd isotopic data is available for these sediments (Wang et al. 2013b). Therefore, we use the $^{147}Sm/^{144}Nd$ versus $\varepsilon_{Nd}(t)$ diagram (Fig. 10b) to evaluate whether pre-Permian metasediments were mixed into the magma source of these granites. It shows that most samples plot between the arc volcanic rocks/Kangding Complex and the Triassic sediments (Fig. 10b). Therefore, it's reasonable to propose that the magma source for these granites was a mixture of arc volcanic rocks/the Kangding Complex and metasediments from the basement, similar in composition to the Zhongza massif.

It is important to distinguish the arc volcanic rocks from the Kangding Complex, which could be the mafic end-member source for the I-type granites in the EYAB. Because, if the mafic end-member was the Kangding Complex, then there may be an ancient basement beneath the EYAB constituting a continental margin arc, or alternatively, it may have been an island arc in the Late Triassic. We consider the Kangding Complex as the mafic end-member for several reasons. Firstly, although the Kangding Complex has similar $\varepsilon_{Nd}(t)$ values to those of the arc volcanic rocks, its initial $^{87}Sr/^{86}Sr$ values show a greater range than those of the arc volcanic rocks (Fig. 10a), which is consistent with those of the I-type granites. Secondly, the whole-rock Pb isotopes of the I-type granites plot much closer to the region of the Songpan-Garzê granites than the arc volcanic rocks (Fig. 11). Thirdly, it is plausible to suggest that the most mafic rocks (samples from the Sucuoma pluton) of the I-type granites in this study could represent rocks that were mainly derived from the mafic end-member and they will inherit some geochemical features from their source. The arc volcanic rocks in the YAB generally show high Sr/Y and $(La/Yb)_N$ with adakitic characteristics (Wang et al., 2011). However, these adakitic features were not observed in the samples from the Sucuoma pluton (Fig.8 a, b). Fourthly, the Late Triassic I-type granites are exposed over a huge area in the EYAB (Fig. 2a). However, the arc volcanic rocks are distributed in a relatively narrow belt to the west of the I-type granites (Fig. 2a), and they show no spatial correlation in the region. Finally, our recent study on the inherited zircons from the Garzê-Daocheng granitic belt further indicate that the existing of an ancient basement that similar to the Kangding Complex beneath the EYAB (Wu et al., 2016b). Therefore, it is possible that the magma source of the I-type granites in the EYAB was a mixture of the Proterozoic Kangding Complex and metasediments from the basement, similar in composition to rocks of the Zhongza massif.

6.3.2 S-type granites

S-type granites are considered to be produced by partial melting of metasedimentary/supracrustal rocks (Chappell and White, 1992), and it is noted that samples from the Ajisenduo pluton plot close to the Triassic sediments in the $\varepsilon_{Nd}(t)$ - $^{147}Sm/^{144}Nd$ diagram (Fig. 10b). Additionally, all the samples from this pluton exhibit high Ca_2O/Na_2O ratios (0.6 - 0.9), and fall into the region of clay-poor metagreywacke source rocks (Fig. 9d). Combined with the relatively large range of $\varepsilon_{Hf}(t)$ (-11.9 to -4.8) and the discussion above, we suggest that the S-type granites of the Ajisenduo pluton were mainly derived from partial melting of metasediments from the basement, with only limited mixture with meta-basaltic rocks from the Kangding Complex.

6.4 Constraints on the evolutionary history of the Yidun arc belt

The EYAB consists, from north to south, of Changtai, Xiangcheng and Zhongdian arcs (Fig.2d). Hou et al. (2003, 2004) pointed out that the Changtai arc was developed on relatively thin crust (20 - 23 km; Hou et al., 1995) and contains widespread Late Triassic bimodal volcanic suites, with arc-type volcanic rocks hosting multiple sulfide deposits (Hou et al., 2003), including the Gacun large Ag-polymetallic VMS deposit and some small Ag-Pb-Zn occurrences, whereas the Zhongdian arc was developed on relatively thicker crust and is characterized by calc-alkaline andesitic-dacitic volcanic rocks and associated porphyry complexes that contain several porphyry-type or skarn-type Cu-polymetallic deposits (Hou et al., 2007). Hou et al. (2004) also proposed that these different features between the Changtai and Zhongdian arc might be caused by variations in subduction angle.

Recently, the adakitic affinity of the calc-alkaline andesitic-dacitic volcanic rocks and associated porphyry complexes in the Zhongdian arc has been recognized and the tectonic setting of this area is relatively well documented (Wang et al., 2011; Leng et al, 2012, 2014). However, subduction of the Garzê-Litang oceanic slab and arc-forming processes during the Late Triassic in the Changtai and Xiangcheng arc are still poorly understood. It is very important to decipher the geodynamic setting of the EYAB (especially the Changtai and Xiangcheng arcs) not only for constraining the evolutionary history of the whole of the YAB but for understanding the distinct ore-forming setting.

Hou and co-workers (2001) summarized previous studies and established a time-frame for granites in the EYAB. However, the geochronological data they used were mostly Rb-Sr and K-Ar isotopic ages, which are easily affected by later geological processes. Moreover, the locations of most samples were not available. This restricts our understanding of the spatial and temporal distribution of magmatism, as well as potential mantle-crust interaction beneath the EYAB in the Late Triassic. In recent years, abundant U-Pb zircon data have been reported (Fig. 12), which allow us to further constrain the evolutionary history of the YAB. Here we focus on magmatism in the Late Triassic. The new precise in situ zircon U-Pb dating results (including this study) indicate there is a dominant peak at ~216 Ma (Fig. 12b). Moreover, it seems that the ages become younger eastward towards the Garzê-Litang suture zone (Fig. 12a). Although different models have been proposed, it is widely accepted that the Garzê-Litang oceanic lithosphere subducted westwards to form the YAB in the Late Triassic (Hou et al. 2001, 2003, 2004; Wang et al., 2011, 2013a; Leng et al., 2014). Hence, slab roll-back can explain the spatial and temporal distribution of magmatim in the EYAB.

Additionally, in the northern EYAB (Changtai arc) the distance between the volcanic arc belt and the Garzê-Litang suture zone is greater than in the southern ETAB (Zhongdian arc; Fig. 2a). Previous studies have demonstrated that although geological processes can show strong diversity between subduction zones, the arc is typically located along a relatively narrow zone where the depth to the slab is around 100 km (Jarrard, 1986; Tatsumi and Eggins, 1995; England et al., 2004). This is also consistent with the research of Keken et al. (2011), in which they noticed that most slabs produce a large burst of fluid around 80 km, based on the study of 56 subduction zones. Combined with the kinematic parameters of slab dip and convergence rate, the location of mantle wedge melting and the position of arc volcanoes can be accurately predicted (Grove et al., 2009). Therefore, in the southern EYAB (Zhongdian arc), rocks of adakitic affinity are much closer to the Garzê-Litang suture zone, possibly the result of steeper subduction of the oceanic slab. On the other hand, according to Hou et al. (1995, 2004), the northern EYAB (Changtai arc) was developed on thin crust (20-23 km), which might account for the more gentle subduction angle of the oceanic slab than for the southern one. Moreover, the huge granitic plutons that are distributed parallel to the Garzê-Litang suture zone in the NYAB likely reflect an environment of high heat flow. As discussed above, the new zircon U-Pb dating shows there is a dominant peak at ~216 Ma (Figs. 12b, 13). After study of the Late Triassic porphyritic intrusions and associated volcanic rocks from the Shangri-La Region, SYAB, Wang et al. (2011) suggested slab break-off occurred at ~216 Ma. Hence, it is reasonable to suggest that the Garzê-Litang oceanic slab broke off and caused upwelling of hot asthenosphere below the lower crust and resulted in subsequent crustal extension at around 216 Ma. Combined with the relatively thin crust, the upwelling of hot asthenosphere would produce a low-pressure, high-temperature environment with relatively water-rich conditions in the northern EYAB (Changtai arc). The thin crust would then experience a high degree of partial melting and produced large volumes of granitic magma.

Our study also sheds light on the basement of the EYAB. As there is a lack of ancient materials exposed in the EYAB, it is impossible to study the basement directly, but the granites provide an alternative way. The isotopic compositions (including Sr-Nd-Hf-Pb isotopes) of the granitic plutons in this study suggest they were derived from a mixture of the Proterozoic Kanding Complex and metasediments from the basement, similar in composition to rocks of the Zhongza massif. It has been proposed that the Zhongza massif rifted from the western Yangtze Craton during the opening of the Garzê-Litang Ocean in the late Palaeozoic (Mo et al., 1993; Pan et al., 1997; Hou et al., 2003). Thus, it is plausible to suggest that the EYAB was developed on an ancient basement similar to the western Yangtze Craton, i.e. it was a continental margin arc rather than was an island arc.

6.5 Tectonic model

Before introducing our tectonic model, we need to summarize the in situ zircon U-Pb dating results from the Jiangda-Weixi belt (JWB; Fig. 2), which lies to the western YAB, that were reported by various authors (see Table. S4) in recent years. The rocks exhibit three peaks, i.e. at ~265 Ma, ~248 Ma and ~235 Ma (Fig. 13a) that correspond to subduction, continental-continental collision and subsequent post-collisional extension, respectively, and possibly slab break-off events in the JWB (Wang et al., 2013c; Zi et al., 2013). In the YAB, our new geochronological data, combined with previous research (Hou et al., 1995; Wang et al., 2011), suggest that the earliest arc magmatism occurred at ~235 Ma, similar to the final event in the JWB. Thus, the two terranes show a close relationship at this time. We therefore propose a new model to explain the evolutionary history of the YAB in the Middle-Late Triassic (Fig. 14).

Between 249 - 235 Ma, collision occurred between the Qiangtang block and the Zhongza massif, followed by post-collisional extension. This process was likely driven by westward subduction of the Garzê-Litang oceanic slab. At the end of this stage, arc magmatism occurred (Fig. 14a).

Between 235 - 220 Ma, the Garzê-Litang oceanic slab rolled back, triggering upwelling of the asthenosphere and lithospheric thinning of the Changtai arc, resulting in the formation of back-arc basin volcanic rocks and the timing of magmatism grew younger towards the trench (Fig. 14b).

Between ~220 - 216 Ma, the oceanic basin closed, followed by slab break off, and resulted in upwelling of hot asthenosphere to form the main component of the Garzê-Daocheng granitic plutons in the EYAB through crustal melting (Fig. 14c).

6. Conclusions

(1) The Sucuoma, Ajisenduo, Jiaduocuo, Cuojiaoma, Maxionggou, Dongcuo and Daocheng granitoids occur in a N-S trending granitic belt in the eastern Yidun arc

belt (EYAB). They were emplaced between 235-218 Ma and show an eastward temporal migration.

(2) Most of the granitic rocks are I-type granites and the magma source was a mixture of the Proterozoic Kangding Complex and metasedimentary rock from the basement. However, rocks of the Ajisenduo pluton are S-type granites that were mainly derived from partial melting of metasediments from the basement, with limited mixture with meta-basaltic rocks from the Kangding Complex.

(3) Slab roll-back, with subsequent slab break-off, model can explain the origin of all these granitic plutons.

Acknowledgments: This work was supported by the China Geological Survey (Grant 1212011121270) and China Postdoctoral Science Foundation funded project (2015M581921). We are grateful for the constructive comments by two anonymous reviewers and Editor Sun-Lin Chung. We thank Liu Yingyuan and Fan Juncheng for their help with the field work.

References

Altherr, R., Holl, A., Hegner, E., Langer, C., Kreuzer, H., 2000. High-potassium, calc-alkaline I-type plutonism in the European Variscides: northern Vosges (France) and northern Schwarzwald (Germany). Lithos 50, 51-73.

BGMRSP, Bureau of Geology and Mineral Resources of Sichuan Province, 1991.

Regional geology of Sichuan Province Geological Memoirs of PRC Ministry of Geology and Mineral Resources, Series 123. Geological Publishing House, Beijing, pp. 1-730 (in Chinese with English summary).

Chappell, B.W., White, A.J.R., 1992. I- and S-type granites in the Lachlan Fold Belt. Transactions of the Royal Society of Edinburgh: Earth Sciences 83, 1-26.

Chen, B.W., Wang, K.Y., Liu, W. J., Cai, Z. J., Zhang, Q.W., Peng, X.J., Qiu, Y.Z., Zheng, Y.Z., 1987. Geotectonics of the Nujiang - Lancangjiang - Jinshajiang Region. Geological Publishing House, Beijing. 204 pp (in Chinese).

Chen, Y.L., Luo, Z.H., Liu, C., 2001. New recognition of Kangding-Mianning metamorphic complexes from Sichuan, western Yangtze Craton. Earth Science-Journal of China University of Geosciences 26, 279-285 (in Chinese with English abstract).

England, P., Engdahl, R., Thatcher, W., 2004. Systematic variation in the depths of slabs beneath arc volcanoes, Geophysical Journal International 156, 377-408.

Gao, R., Xiao, L., He, Q., Yuan, J., Ni, P.Z., Du, J.X., 2010. Geochronology, Geochemistry and Petrogenesis of Granites in Weixi - Deqin, West Yunnan. Earth Science-Journal of China University of Geosciences 35, 186-200 (in Chinese with English abstract).

Grove, T.L., Till, C.B., Lev, E., Chatterjee, N., Medard, E., 2009. Kinematic variables and water transport control the formation and location of arc volcanoes. Nature 459, 694 - 697.

He, D.F., Zhu, W.G., Zhong, H., Ren, T., Bai, Z.J., Fan, H.P., 2013. Zircon U-Pb geochronology and elemental and Sr–Nd–Hf isotopic geochemistry of the Daocheng granitic pluton from the Yidun Arc, SW China. Journal of Asian Earth Sciences 67-68, 1-17.

Hou, Z.Q., Mo, X.X., 1991. The evolution of Yidun island arc and implications in the exploration of Kuroko-type volcanogenic massive sulphide deposits in Sanjiang area, China. Earth Science-Journal of China University of Geosciences 16, 153-164 (in Chinese with English abstract).

Hou, Z.Q., Hou, L.W., Ye, Q.T., Liu, F.L., Tang, G.G., 1995. Tectono-Magmatic Evolution and Volcanogenic Massive Sulphide Deposits in the Yidun Island-Arc, Sanjiang Region, China. In Earthquake Publishing House, Beijing, pp 1-218 (in Chinese).

Hou, Z.Q., Qu, X.M., Yang, Y.Q., 2001. Collision orogeny in the Yidun arc: evidence from granites in the Sanjiang region, China. Acta Geologica Sinica 75, 484-497 (in Chinese with English abstract).

Hou, Z.Q., Yang, Y.Q., Wang, H.P., Qu, X.M., Lv, Q.T., Huang, D.H., Wu, X.Z., Yu, J.J., Tang, S.H., Zhao, J.H., 2003. Collision-Orogenic Processes and Mineralization Systems of the Yidun Arc. Geological Publishing House, Beijing. 345 pp (in Chinese).

Hou, Z.Q., Yang, Y.Q., Qu, X.M., Huang, D.H., Lv, Q.T., Wang, H.P., Yu, J.J., Tang, S.H., 2004. Tectonic evolution and mineralization systems of the Yidun arc orogen in Sanjiang region, China. Acta Geologica Sinica 78, 109-120 (in Chinese with English abstract).

Hou, Z.Q., Zaw, K., Pan, G.T., Mo, X.X., Xu, Q., Hu, Y.Z., Li, X.Z., 2007. Sanjiang Tethyan metallogenesis in SW China: Tectonic setting, metallogenic epochs and deposit types. Ore Geology Reviews 31, 48-87.

Hu, Z.C., Liu, Y.S., Gao, S., Liu, W.G., Zhang, W., Tong, X.R., Lin, L., Zong, K.Q., Li, M., Chen, H.H., Zhou, L., Yang, L., 2012. Improved in situ Hf isotope ratio analysis of zircon using newly designed X skimmer cone and jet sample cone in combination with the addition of nitrogen by laser ablation multiple collector ICP-MS. Journal of Analytical Atomic Spectrometry 27, 1391-1399.

Jarrard, R.D., 1986. Relations among subduction parameters. Reviews of Geophysics 24, 217-284.

Keken, P. E.V., Hacker, B.R., Syracuse, E.M, Abers, G.A., 2011. Subduction factory: 4. Depth-dependent flux of H_2O from subducting slabs worldwide. Journal of Geophysical Research 116, B01401.

Leng, C.B., Zhang, X.C., Hu, R.Z., Wang, S.X., Zhong, H., Wang, W.Q., Bi, X.W., 2012. Zircon U-Pb and molybdenite Re-Os Geochronology and Sr-Nd-Pb-Hf isotopic constraints on the genesis of the Xuejiping porphyry copper deposit in Zhongdian, Northwest Yunnan, China. Journal of Asian Earth Sciences 60, 31-48.

Leng, C.B., Huang, Q.Y., Zhang, X.C., Wang S.X., Zhong, H., Hu, R.Z., Bi, X.W., Zhu, J.J., Wang., S.X., 2014. Petrogenesis of the Late Triassic volcanic rocks in the Southern Yidun arc, SW China: Constraints from the geochronology, geochemistry, and Sr-Nd-Pb-Hf isotopes. Lithos 190-191, 363-382.

Li, X.H., Liu, D.Y., Sun, M., Li, W.X., Liang, X.R., Liu, Y., 2004. Precise Sm-Nd and U-Pb isotopic dating of the super-giant Shizhuyuan polymetallic deposit and its host granite, Southeast China. Geological Magazine 141, 225-231.

Liu, C.J., Diao, Z.Z., Zhang, Z.G., 1996. Tethyan Geology of Western Sichuan and Eastern Tibet. Southwest Jiaotong University Press, Chengdu (148 pp., in Chinese with English abstract).

Liu, S.W., Wang, Z.Q., Yan, Q.R., Li, Q.G., Zhang, D.H., 2006. Indosinian tectonic setting of the Southern Yidun Arc: Constraints from SHRIMP zircon chronology and geochemistry of dioritic porphyries and granites. Acta Geologica Sinica (English Edition) 80, 387-399.

Liu, Y.S., Hu, Z.C., Gao, S., Günther, D., Gao, C.G., Chen, H.H., 2008. In situ analysis of major and trace elements of anhydrous minerals by LA-ICP-MS without applying an internal standard. Chemical Geology 257, 34-43.

Liu, Y.S., Hu, Z.C., Zong, K.Q., Gao, C.G., Gao, S., Xu, J., Chen, H.H., 2010. Reappraisement and refinement of zircon U-Pb isotope and trace element analyses by LA-ICP-MS. Chinese Science Bulletin 55, 1535-1546.

Metcalfe, I., 2011. Tectonic framework and Phanerozoic evolution of Sundaland. Gondwana Research 19, 3-21.

Mo, X.X., Lu, F.X., Shen, S.Y., Zhu, Q.W., Hou, Z.Q., Yang, K.H., Deng, J.F., Liu, X.P., He, C.X., 1993. Sanjiang Tethyan Volcanism and Related Mineralization. Geological Publishing House, Beijing. 267 pp (in Chinese with English abstract).

Pan, G.T., Chen, Z.L., Li, X.Z., 1997. Geological-Tectonic Evolution in the Eastern Tethys. Geological Publishing House, Beijing. 218 pp (in Chinese with English abstract).

Patino Douce, A.E., 1999. What do experiments tell us about the relative contributions of crust and mantle to the origin of granitic magmas? In: Castro, A., Fernandez, C., Vjgneress, J.L. (Eds.), Understanding Granites: Integrating New and Classical Techniques. Geological Society London Special Public 168, 55-75.

Peng, T.P., Zhao, G.C., Fan, W.M., Peng, B.X., Mao, Y.S., 2014. Zircon geochronology and Hf isotopes of Mesozoic intrusive rocks from the Yidun terrane, Eastern Tibetan Plateau: Petrogenesis and their bearings with Cu mineralization. Journal of Asian Earth Sciences 80, 18-33.

Qu, X.M., Hou, Z.Q., Zhou, S.G., 2002. Geochemical and Nd, Sr isotopic study of the post-orogenic granites in the Yidun arc belt of northern Sanjiang region, southwestern China. Resource Geology 52, 163-172.

Reid, A.J., Wilson, C.J.L., Phillips, D., Liu, S., 2005. Mesozoic cooling across the Yidun Arc, central-eastern Tibetan Plateau: A reconnaissance Ar^{40}/Ar^{39} study. Tectonophysics 398, 45-66.

Reid, A., Wilson, C.J.L., Shun, L., Pearson, N., Belousova, E., 2007. Mesozoic plutons of the Yidun Arc, SW China: U/Pb geochronology and Hf isotopic signature. Ore Geology Reviews 31, 88-106.

Roger, F., Jolivet, M., Malavieille, J., 2008. Tectonic evolution of the Triassic fold belts of Tibet. Comptes Rendus Geoscience 340, 180-189.

Roger, F., Jolivet, M., Malavieille, J., 2010. The tectonic evolution of the Songpan-Garze (North Tibet) and adjacent areas from Proterozoic to present: a synthesis. Journal of Asian Earth Sciences 39, 254-269.

Song, X.Y., Zhou, M.F., Cao, Z.M., Robinson, P.T., 2004. Late Permian rifting of the South China Craton caused by the Emeishan mantle plume? Journal of the Geological Society 161, 773-781.

Sun, S.S., McDonough, W.F., 1989. Chemical and isotopic systematics of oceanic basalts: implications for mantle composition and processes. In: Saunders, A.D., Norry, M.J. (Eds.), Magmatism in the Ocean Basins. Geological Society, London, Special Publications, 42, 313-345.

Sylvester, P.J., 1998. Post-collisional strongly peraluminous granites. Lithos 45, 29-44.

Tatsumi, Y., Eggins, S.M., 1995. Subduction Zone Magmatism. Blackwell, Cambridge. 211 pp.

Wang, B.Q., Zhou, M.F., Li, J.W., Yan, D.P., 2011. Late Triassic porphyritic intrusions and associated volcanic rocks from the Shangri-La region, Yidun terrane, Eastern Tibetan Plateau: Adakitic magmatism and porphyry copper mineralization. Lithos 127, 24-38.

Wang, B.Q., Zhou, M.F., Chen, W.T., Gao, J.F., Yan, D.P., 2013a. Petrogenesis and tectonic implications of the Triassic volcanic rocks in the northern Yidun Terrane, Eastern Tibet. Lithos 175-176, 285-301.

Wang B.Q., Wang W, Zhou M.F., 2013b. Provenance and tectonic setting of the Triassic Yidun Group, the Yidun Terrane, Tibet. Geoscience Frontiers 4: 765-777.

Wang, B.D., Wang, L.Q., Wang, D.B., Zhang, W.P., 2011. Zircons U-Pb dating of volcanic rocks from Renzhixueshan Formation in Shangdie rift basin of Sanjiang area and its geological implications. Acta Petrologica et Mineralogica 30, 25-33 (in Chinese with English abstract).

Wang, B.D., Wang, L.Q., Chen, J.L., Yin, F.G., Wang, D.B., Zhang, W.P., 2013c. Triassic three-stage collision in the Paleo-Tethys: Constraints from magmatism in the Jiangda - Deqen - Weixi continental margin arc, SW China. Gondwana Research 26, 475-491.

Wang, X.F., Metcalfe, I., Jian, P., He, L.Q., Wang, C.S., 2000. The Jinshajiang - Ailaoshan Suture Zone, China: tectonostratigraphy, age and evolution. Journal of Asian Earth Sciences 18, 675-690.

Wei, G.J., Liang, X.R., Li, X.H., Liu, Y., 2002. Precise measurement of Sr isotopic compositions of liquid and solid base using (LP) MC-ICP-MS. Geochimica 31, 295-299 (in Chinese with English abstract).

Whalen, J.B., Currie, K.L., Chappell, B.W., 1987. A-type granites: geochemical characteristics, discrimination and petrogenesis. Contributions to Mineralogy and Petrology 95, 407-419.

Wu, T., Xiao, L., Ma, C.Q., Huang, W., 2013. The geochronological, geochemical and Sr-Nd isotopic characteristics of Tongpu intrusive complex and its implications. Acta Petrologica Sinica 29, 2567-3580 (in Chinese with English abstract).

Wu, T., Xiao, L., Gao, R., Yang, H.J., Yang, G., 2014a. Petrogenesis and tectonic setting of the Queershan composite granitic pluton, eastern Tibetan Plateau: Constraints from geochronology, geochemistry and Hf isotope data. Science China Earth Sciences 57, 2712-2725.

Wu, T., Xiao, L., Ma, C.Q., Pirajno, F., Sun, Y., Zhan, Q.Y., 2014b. A mafic intrusion of "arc affinity" in a post-orogenic extensional setting: A case study from Ganluogou gabbro in the northern Yidun Arc Belt, eastern Tibetan Plateau. Journal of Asian Earth Sciences 94, 139-156.

Wu, T., Xiao, L., Wilde, S.A., Ma, C.Q., Li, Z.L., Sun, Y., Zhan, Q.Y., 2016a. Zircon U-Pb age and Sr-Nd-Hf isotope geochemistry of the Ganluogou dioritic complex in the northern Triassic Yidun arc belt, Eastern Tibetan Plateau: Implications for the closure of the Garzê-Litang Ocean. Lithos 248-251, 94-108.

Wu, T., Xiao, L., Ma, C. Q., 2016b. The U-Pb geochronology of detrital and inherited zircons in the Yidun arc belt, eastern Tibet Plateau and its tectonic implications. Journal of Earth Science 27, 461-473.

Xiao, L., Zhang, H.F., Clemens, J.D., Wang, Q.W., Kan, Z.Z., Wang, K.M., Ni, P.Z., Liu, X.M., 2007. Late Triassic granitoids of the eastern margin of the Tibetan Plateau: Geochronology, petrogenesis and implications for tectonic evolution. Lithos 96, 436-452.

Xiao, L., He, Q., Pirajno, F., Ni. P.Z., Du, J.X., Wei, Q.R., 2008. Possible correlation between a mantle plume and the evolution of Paleo-Tethys Jinshajiang Ocean: Evidence from a volcanic rifted margin in the Xiaru-Tuoding area, Yunnan, SW China. Lithos 100, 112-126.

Yan, Q.R., Wang, Z.Q., Liu, S.W., Li, Q.G., Zhang, H.Y., Wang, T., Liu, D.Y., Shi, Y.R., Jian, P., Wang, J.G., Zhang, D.H., Zhao, J., 2005. Opening of the Tethys in southwest China and its significance to the breakup of East Gondwanaland in late Paleozoic: Evidence from SHRIMP U-Pb zircon analyses for the Garzê ophiolite block. Chinese Science Bulletin 50, 256-264.

Zartman, R.E., Doe, B.R., 1981. Plumbotectonics -the model. Tectonophysics 75, 135-162.

Zhang, Z.M., Jin, M., 1979. Two kinds of mélange and their tectonic significance in Xiangcheng-Derong area, southwestern. Sichuan. Scientia Geologica Sinica 3, 223-228 (in Chinese).

Zhang, H.F., Zhang, L., Harris, N., Jin, L.L., Yuan, H.L., 2006. U-Pb zircon ages, geochemical and isotopic compositions of granitoids in Songpan-Garze fold belt, eastern Tibetan Plateau: constraints on petrogenesis and tectonic evolution of the basement. Contributions to Mineralogy and Petrology 152, 75-88.

Zhang, W.P., Wang, L.Q., Wang, B.D., Wang, D.B., Dai, J., Liu, W., 2011. Chronology, geochemistry and petrogenesis of Deqin granodiorite body in the middle section of Jiangda-Weixi arc. Acta Petrologica Sinica 22, 2577-2590 (in Chinese with English abstract).

Zhao, X.F., Zhou, M.F., Li, J.W. Wu, F.Y., 2008. Association of Neoproterozoic A- and I-type granites in South China: Implications for generation of A-type granites in a subduction-related environment. Chemical Geology 257, 1-15.

Zhou, M.F., Yan, D.P., Kennedy, A.K., Li, Y., Ding, J., 2002. SHRIMP U-Pb zircon geochronological and geochemical evidence for Neoproterozoic arc-magmatism along the western margin of the Yangtze Block, South China. Earth and Planetary Science Letters 196, 51-67.

Zi, J.W., Cawood, P.A., Fan, W.M., Tohver, E., Wang, Y.J., McCuaig, T.C., 2012a. Generation of Early Indosinian enriched mantle-derived granitoid pluton in the Sanjiang Orogen (SW China) in response to closure of the Paleo-Tethys. Litho 140-141, 166-182.

Zi, J.W., Cawood, P.A., Fan, W.M., Wang, Y.J., Tohver, E., McCuaig, T.C., Peng, T.P., 2012b. Triassic collision in the Paleo-Tethys Ocean constrained by volcanic activity in SW China. Lithos 144, 145-160.

Zi, J.W., Cawood, P.A., Fan, W.M., Tohver, E., Wang, Y.J., McCuaig, T.C., Peng, T.P., 2013. Late Permian-Triassic magmatic evolution in the Jinshajiang orogenic belt, SW China and implications for orogenic processes following closure of the Paleo-Tethys. American Journal of Science 313, 81-112.

Zhu, J.J., Hu, R.Z., Bi, X.W., Zhong, H., Chen, H., 2011. Zircon U-Pb ages, Hf-O isotopes and whole-rock Sr-Nd-Pb isotopic geochemistry of granitoids in the Jinshajiang suture zone, SW China: Constraints on petrogenesis and tectonic evolution of the Paleo-Tethys Ocean. Lithos 126, 248-264.

Figure Captions

Fig.1 (a) Sketch map highlighting Paleo-Tethys sutures and associated magmatic arcs in the Sanjiang orogenic belt (after Zi et al., 2012a). (b) Tectonic setting of the Sanjiang orogenic belt (after Metcalfe, 2011).

Fig. 2 (a) Simplified geological map of the Yidun Terrane and surrounding areas (after Hou et al., 2001 and Reid et al., 2005). (b) Structural domains of the Yidun Arc (after Reid et al., 2005). (d) Subdivision of northern and southern Yidun Arc.

Fig. 3 Photomicrographs of selected rock samples. (a) Porphyritic monzogranite from the Sucuoma pluton (SCM-7). (b) Granodiorite (SCM-17h) and (c) monzogranite (SCM-10) from the Sucuoma pluton. (d) Monzogranite (ZK-3), (e) granodiorite (JDC-1) and (f) porphyritic monzogranite (CJM-5) from Cuojiaoma pluton. Abbreviations are: Amp, Amphibole; Kf, K-feldspar; Pl, plagioclase; Q, Quartze; Bi, Biotite; Ms, Moscovite.

Fig. 4 U-Pb concordia diagrams and examples of zircon CL images for rock samples from (a), (b) Sucuoma pluton (SCM-10); (c), (d) Ajisenduo pluton (ZK-1); (e), (f) Jiaduocuo pluton (JDC-2); (g), (h) Cuojiaoma pluton (CJM-6); (i), (j), (k), (l) Dongcuo pluton (HZS-8 and HZS-14); (m) Daocheng pluton (DC-9) and (n)

Maxionggou pluton (MXG-1).

Fig. 5 The distribution of $\varepsilon_{Hf}(t)$ vs. Age (Ma) for samples (a) SCM-10, (b) ZK-1, (c) JDC-2 and (d) HZS-8. All the samples were calculated at their formation age. Data source: the Kangding Complex samples are from Zhao et al. (2008); the arc volcanic rocks are from Leng et al. (2012, 2014);

Fig. 6 Selected major and trace elements vs. SiO_2 for the rock samples from the NYAB. (a) MgO vs. SiO_2; (b) Fe_2O_{3t} vs. SiO_2; (c) CaO vs. SiO_2; (d) P_2O_5 vs. SiO_2; (e) K_2O vs. SiO_2; (f) Rb vs. SiO_2.

Fig. 7 (a) A/NK vs. A/CNK diagram for rock sample from the NYAB. (b) A-type granite discrimination diagram for the granites (Whalen et al., 1987), FG: fractionated felsic granites; OGT: unfractionated M-, I- and S-type granites. (c) Plots of P_2O_5 vs. Rb, and (d) Th vs. Rb. The I and S-type trends are from Chappell and White, 1992.

Fig. 8 Primitive-mantle normalized trace element patterns (a, c, e, g, i, k, m) and chondrite-normalized REE patterns (b, d, f, h, j, l, n) of rock samples from Sucuoma, Ajisenduo, Jiacuocuo, Cuojiaoma, Dongcuo, Daocheng, Maxionggou pluons. (Normalization values are from Sun and McDonough, 1989)

Fig. 9 Source discrimination diagrams for rock samples from the NYAB. (a) $Al_2O_3/(MgO+FeO_T)$molar vs. $CaO/(MgO+FeO_T)$molar diagram (after Altherr et al., 2000). (b) $(Na_2O+K_2O)/(FeO+MgO+Ti_2O)$ vs. $Na_2O+K_2O+FeO+MgO+Ti_2O$ diagram (after Patino Douce, 1999). (c) CaO/Na_2O vs. Al_2O_3/TiO_2 and (d) Rb/Ba vs. Rb/Sr diagram (after Sylvester, 1998).

Fig.10 (a) $\varepsilon_{Nd}(t)$ vs. initial $^{87}Sr/^{86}Sr_i$ diagram and (b) $\varepsilon_{Nd}(t)$ vs. $^{147}Sm/^{144}Nd$ diagram for the rock samples from the NYAB. All the data were calculated at t = 216 Ma. Data source: the Kangding Complex samples are from Chen et al. (2001); the arc volcanic rocks are from Wang et al. (2011) and Leng et al. (2012, 2014); the Triassic sediments are from Wang et al. (2013a).

Fig.11 (a) $(^{208}Pb/^{204}Pb)_t$ vs. $(^{206}Pb/^{204}Pb)_t$ diagram. (b) $\varepsilon_{Nd}(t)$ vs. $(^{207}Pb/^{204}Pb)_t$ diagram. (c) $\varepsilon_{Nd}(t)$ vs. $(^{208}Pb/^{204}Pb)_t$ diagram. All the data were calculated at t = 216 Ma. Pb isotopic evolution lines of upper crust, lower crust and mantle are from Zartman and Doe (1981). Data source: Arc volcanic rocks are from Leng et al. (2012, 2014); Songpan - Garzê granites are from Xiao et al. (2007).

Fig. 12 The distribution of U-Pb zircon ages from Triassic igneous rocks in the Yidun arc and (b) their U-Pb age spectra with a peak at ~216 Ma.

Fig. 13 The U-Pb age spectra of igneous rocks in the Jiangda-Weixi arc hich shows three peaks at ~265 Ma, ~248 Ma and ~235 Ma. The references are listed in Table S4.

Fig. 14 A tectonic model showing the evolutionary history of Yidun arc belt in the late Triassic. (a) 249-235 Ma, collision occurred between the Qiangtang block and the Zhongza massif, followed by post-collisional extension. Garzê-Litang oceanic slab subducted westward beneath the Yidun arc belt. (b) 235-220 Ma, slab rolled back had happened, triggering upwelling of the asthenosphere and lithospheric, resulting in the timing of magmatism grew younger towards the trench. (c) ~220-216 Ma, the oceanic basin closed, followed by slab break off, and resulted in upwelling of hot asthenosphere to form the main component of the Garzê-Daocheng granitic plutons in the EYAB through crustal melting.

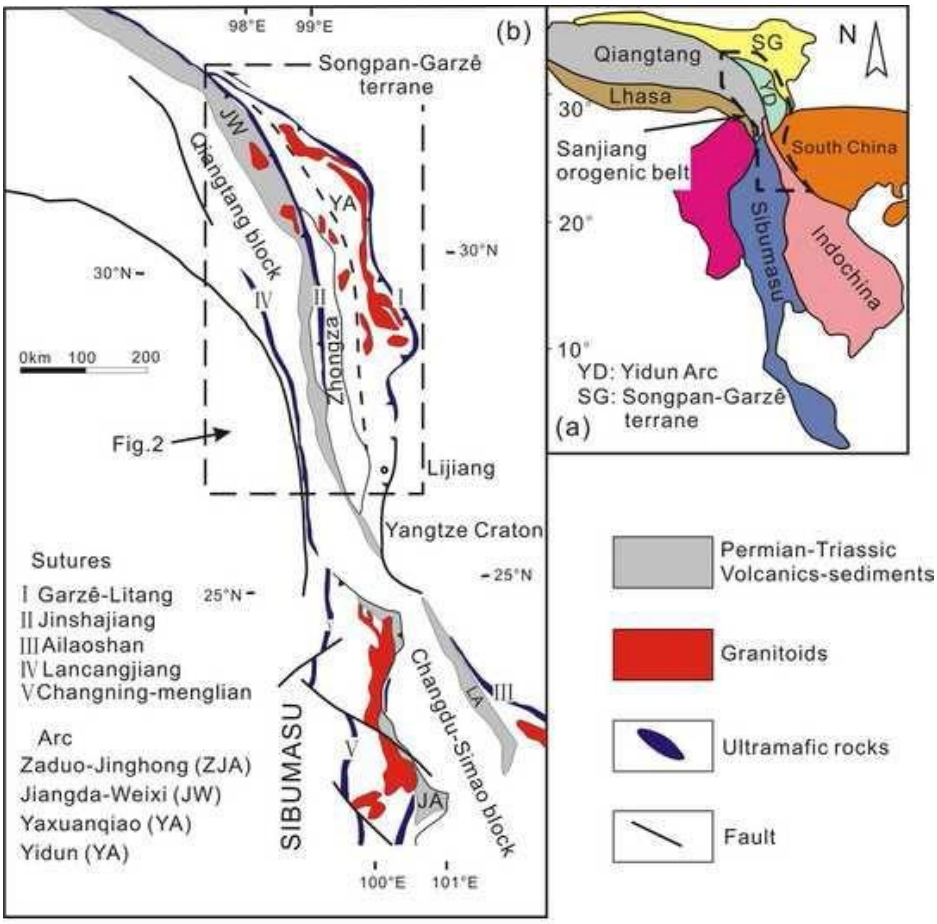

(b)
98°E
99°E
Songpan-Garzê terrane
JW
Changtang block
YA
30°N
IV
II
I
Zhongza
0km 100 200
Fig.2
Lijiang
Yangtze Craton
Sutures
I Garzê-Litang
II Jinshajiang
III Ailaoshan
IV Lancangjiang
V Changning-menglian
Arc
Zaduo-Jinghong (ZJA)
Jiangda-Weixi (JW)
Yaxuanqiao (YA)
Yidun (YA)
25°N
SIBUMASU
Changdu-Simao block
LA
III
V
JA
100°E
101°E
Qiangtang
SG
N
Lhasa
YD
30°
Sanjiang orogenic belt
South China
20°
Sibumasu
Indochina
10°
YD: Yidun Arc
SG: Songpan-Garzê terrane
(a)
Permian-Triassic Volcanics-sediments
Granitoids
Ultramafic rocks
Fault

Fig.1

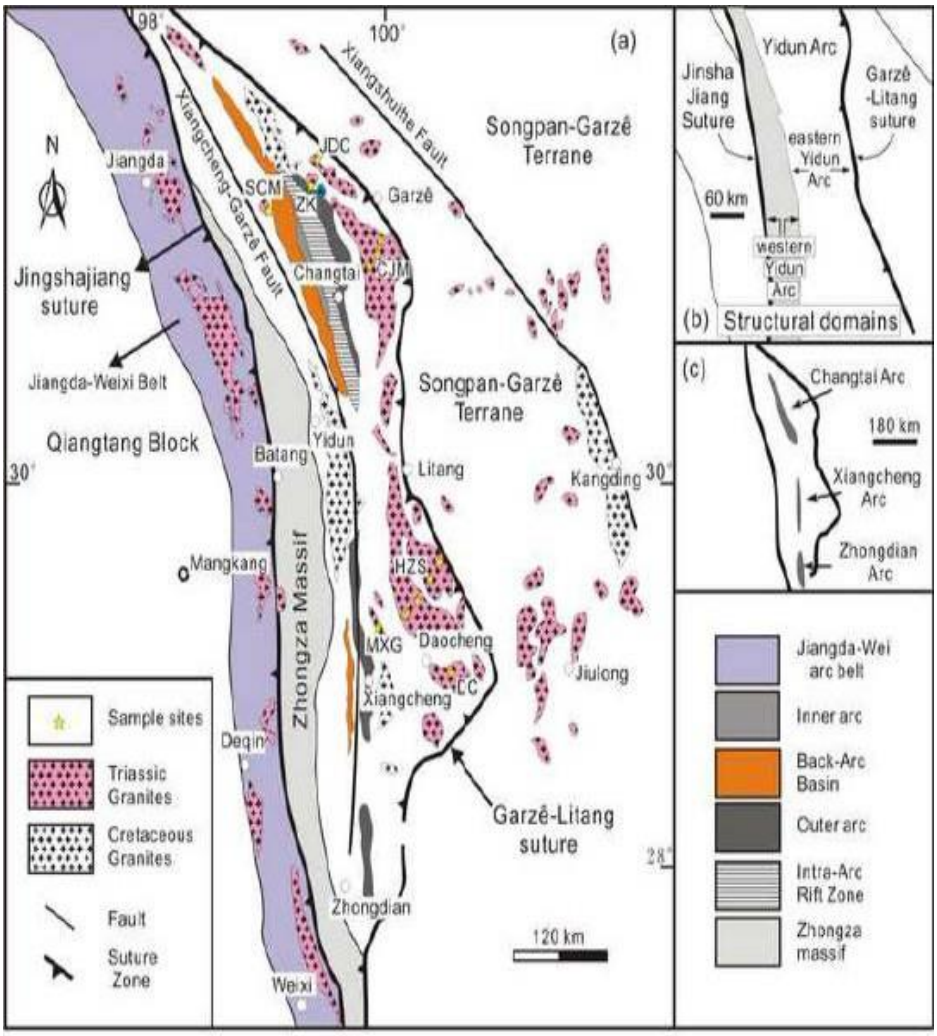
98°
100°
(a)
Xiangshuihe Fault
Xiangcheng-Garzê Fault
Songpan-Garzê Terrane
N
Jiangda
JDC
SCM
ZK
Garzê
Changtai
CJM
Jingshajiang suture
Jiangda-Weixi Belt
Songpan-Garzê Terrane
Qiangtang Block
Batang
Yidun
Litang
Kangding
30°
30°
Mangkang
Zhongza Massif
HZS
MXG
Daocheng
Jiulong
Xiangcheng
CC
Sample sites
Triassic Granites
Cretaceous Granites
Fault
Suture Zone
Deqin
Garzê-Litang suture
28°
Zhongdian
120 km
Weixi
Yidun Arc
Jinsha Jiang Suture
Garzê -Litang suture
eastern Yidun Arc
60 km
western Yidun Arc
(b) Structural domains
(c)
Changtai Arc
180 km
Xiangcheng Arc
Zhongdian Arc
Jiangda-Wei arc belt
Inner arc
Back-Arc Basin
Outer arc
Intra-Arc Rift Zone
Zhongza massif

Fig. 2

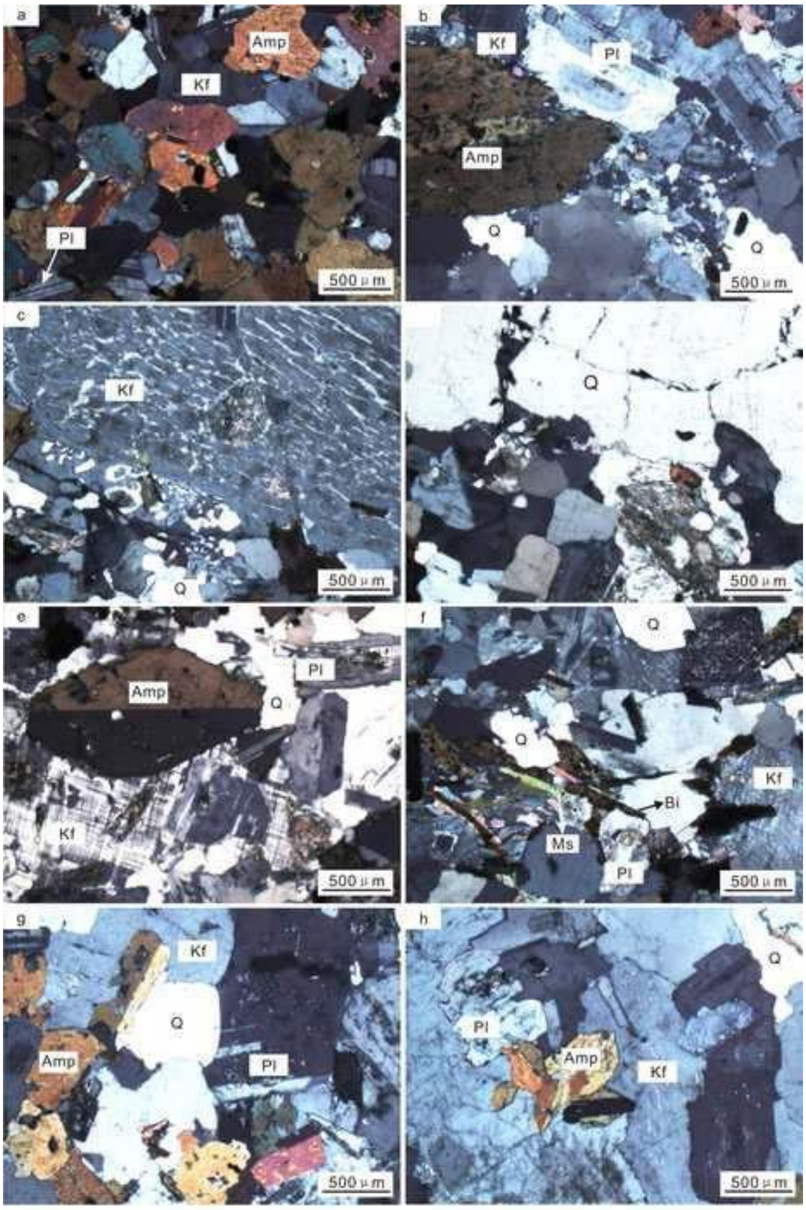
a
Amp
Kf
Pl
500 μm
b
Kf
Pl
Amp
Q
Q
500 μm
c
Kf
Q
500 μm
Q
500 μm
e
Amp
Pl
Q
Kf
500 μm
f
Q
Q
Kf
Bi
Ms
Pl
500 μm
g
Kf
Q
Amp
Pl
500 μm
h
Q
Pl
Amp
Kf
500 μm

Fig.3

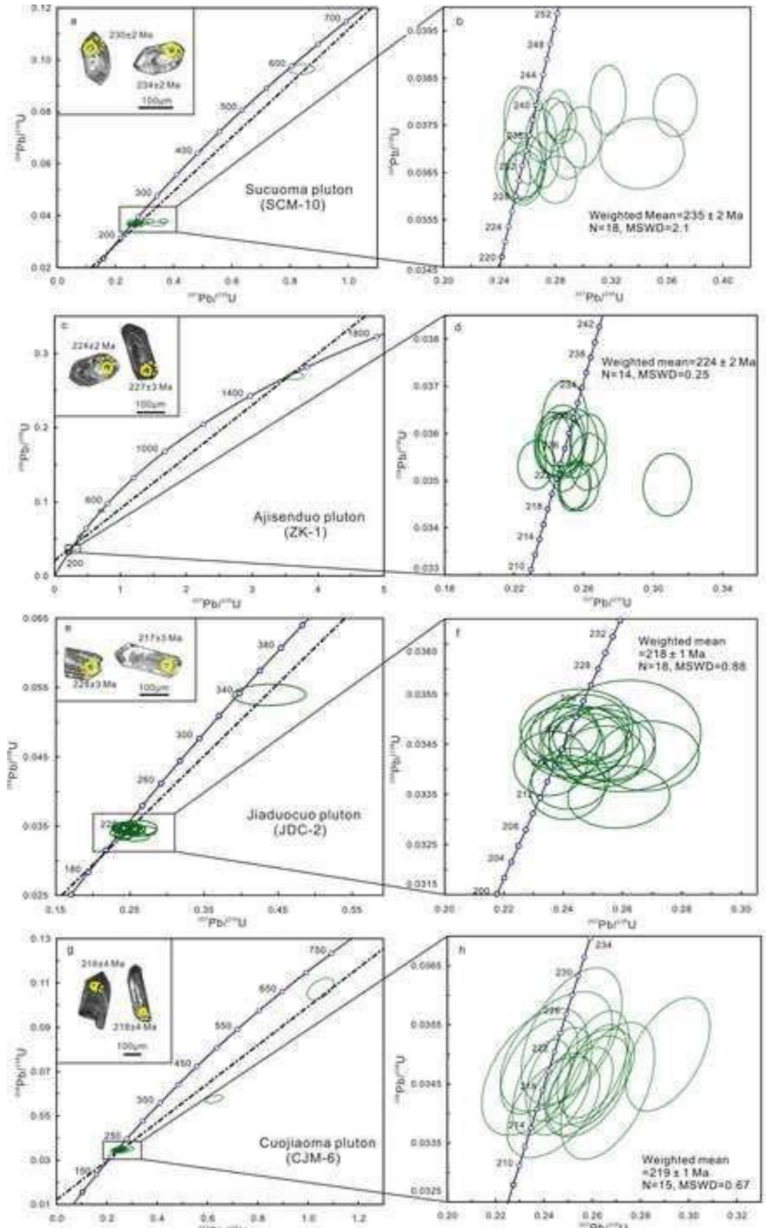
Sucuoma pluton
(SCM-10)
Weighted Mean=235 ± 2 Ma
N=18, MSWD=2.1
Ajisenduo pluton
(ZK-1)
Weighted mean=224 ± 2 Ma
N=14, MSWD=0.25
Jiaduocuo pluton
(JDC-2)
Weighted mean
=218 ± 1 Ma
N=18, MSWD=0.88
Cuojiaoma pluton
(CJM-6)
Weighted mean
=219 ± 1 Ma
N=15, MSWD=0.67

Fig. 4

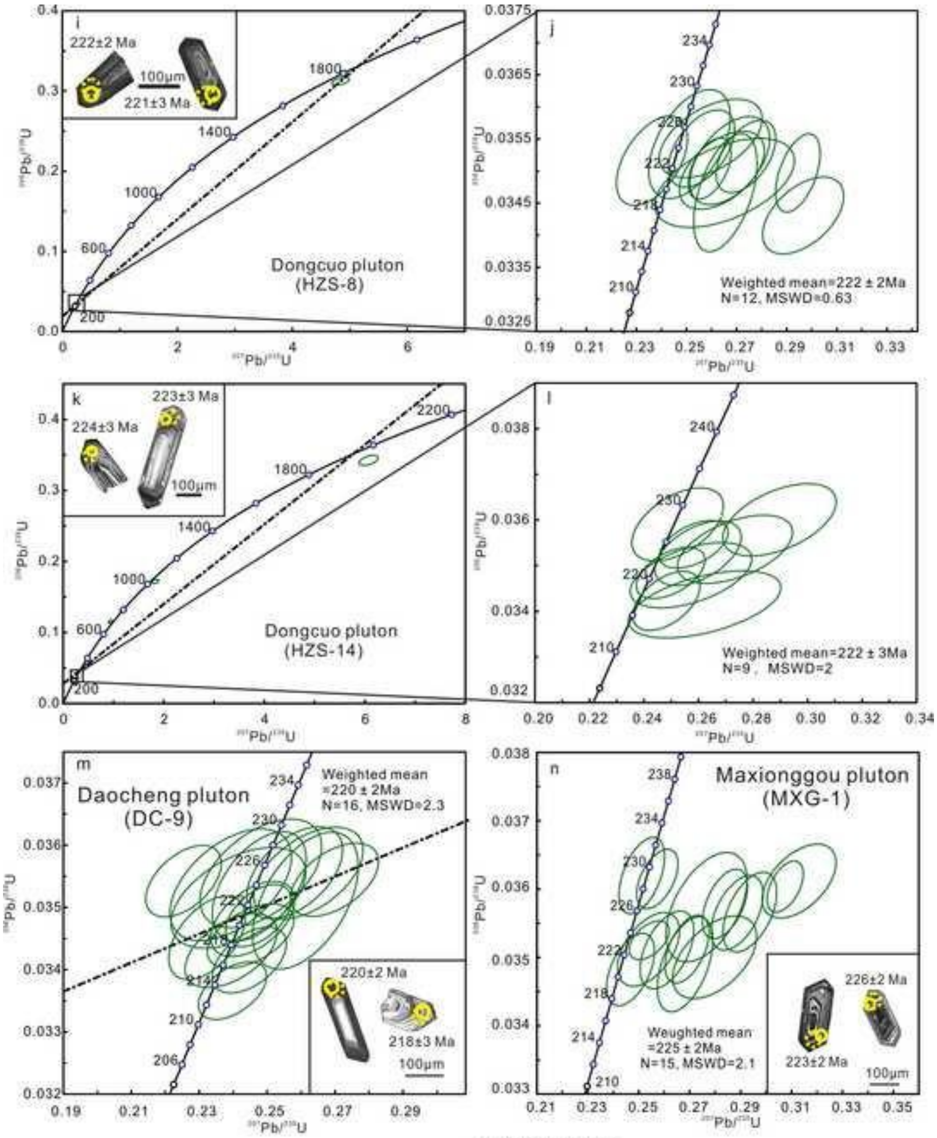

Fig.4 (continued)

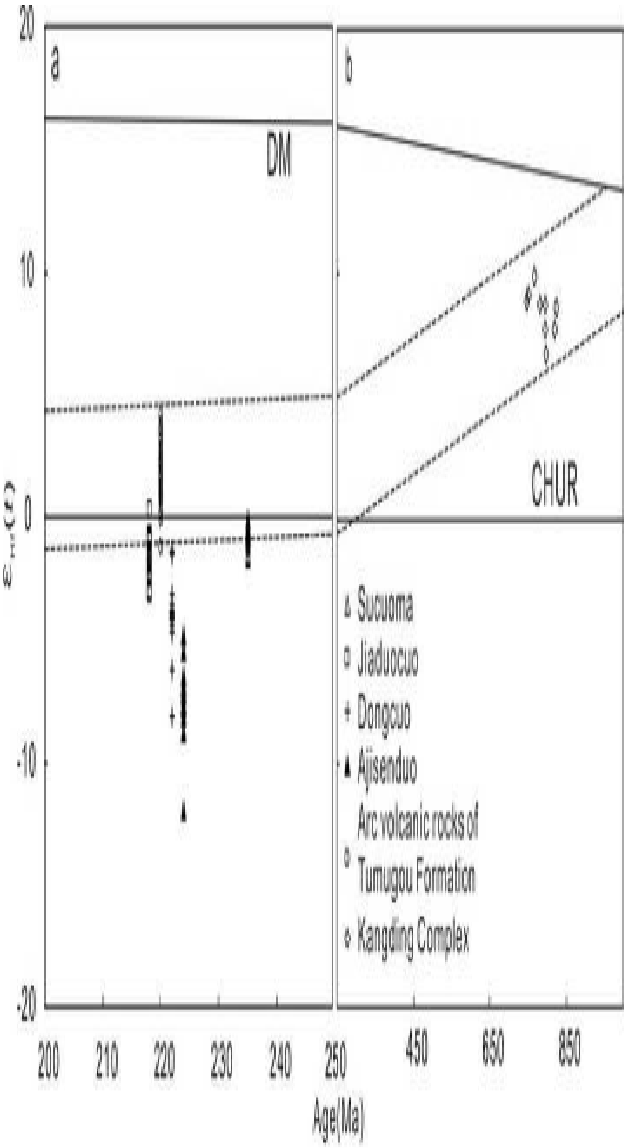
a
b
DM
CHUR
20
10
0
-10
-20
Sucuoma
Jiaduocuo
Dongcuo
Ajisenduo
Arc volcanic rocks of Tumugou Formation
Kangding Complex
200
210
220
230
240
250
450
650
850
Age(Ma)

Fig.5

862

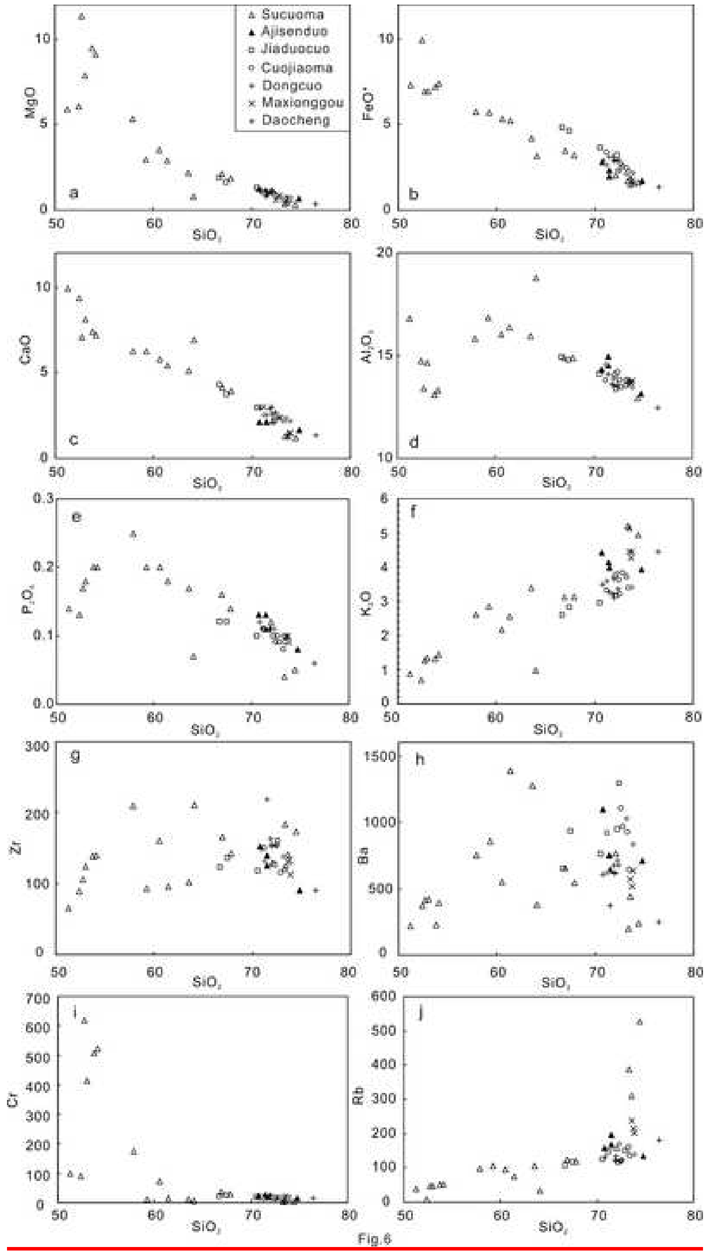
Sucuoma
Ajisenduo
Jiaduocuo
Cuojiaoma
Dongcuo
Maxionggou
Daocheng
MgO
FeO*
CaO
Al2O3
P2O5
K2O
Zr
Ba
Cr
Rb
SiO2
a
b
c
d
e
f
g
h
i
j

Fig.6

863

864
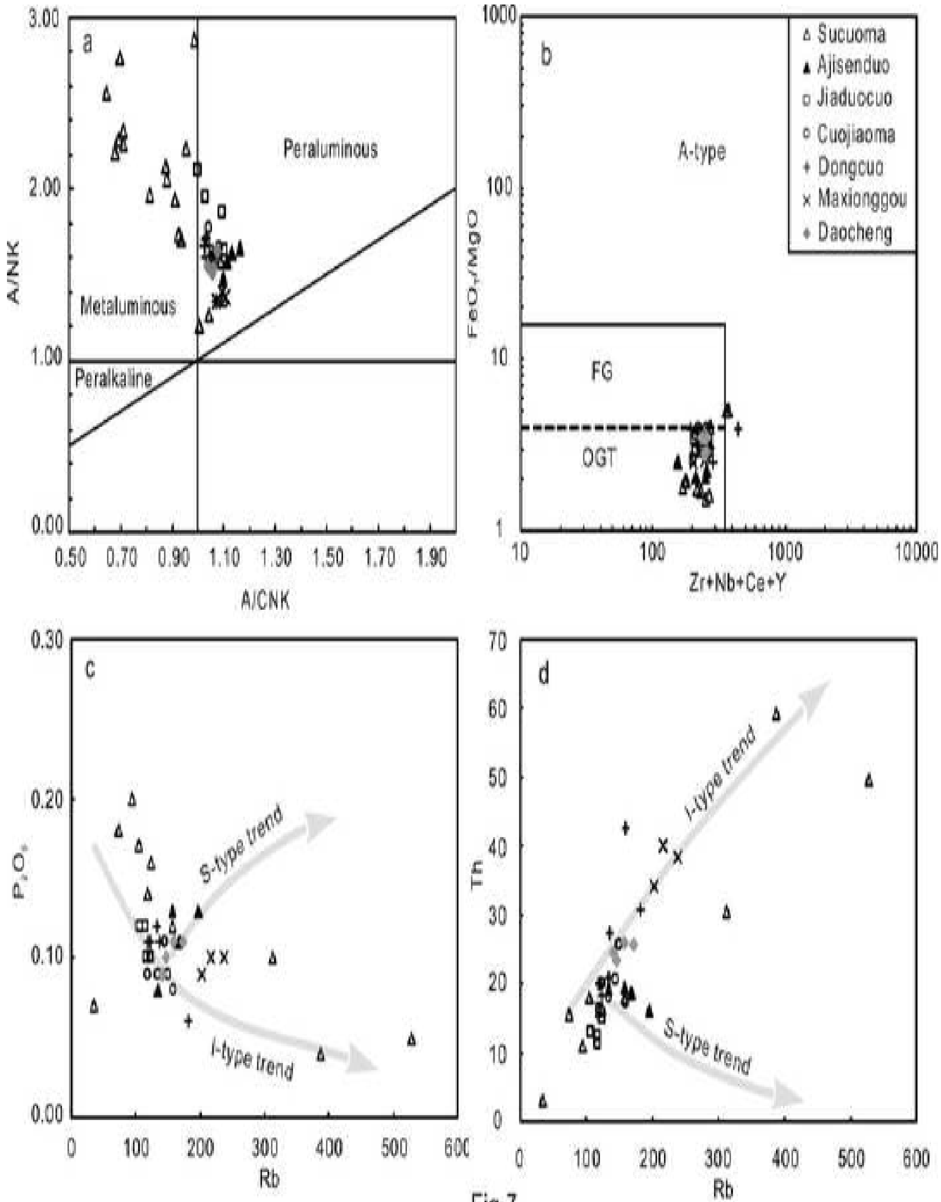
a
b
c
d
A/NK
A/CNK
Peraluminous
Metaluminous
Peralkaline
FeO_T/MgO
Zr+Nb+Ce+Y
A-type
FG
OGT
Sucuoma
Ajisenduo
Jiaduocuo
Cuojiaoma
Dongcuo
Maxionggou
Daocheng
P2O5
Rb
Th
S-type trend
I-type trend

Fig.7

865

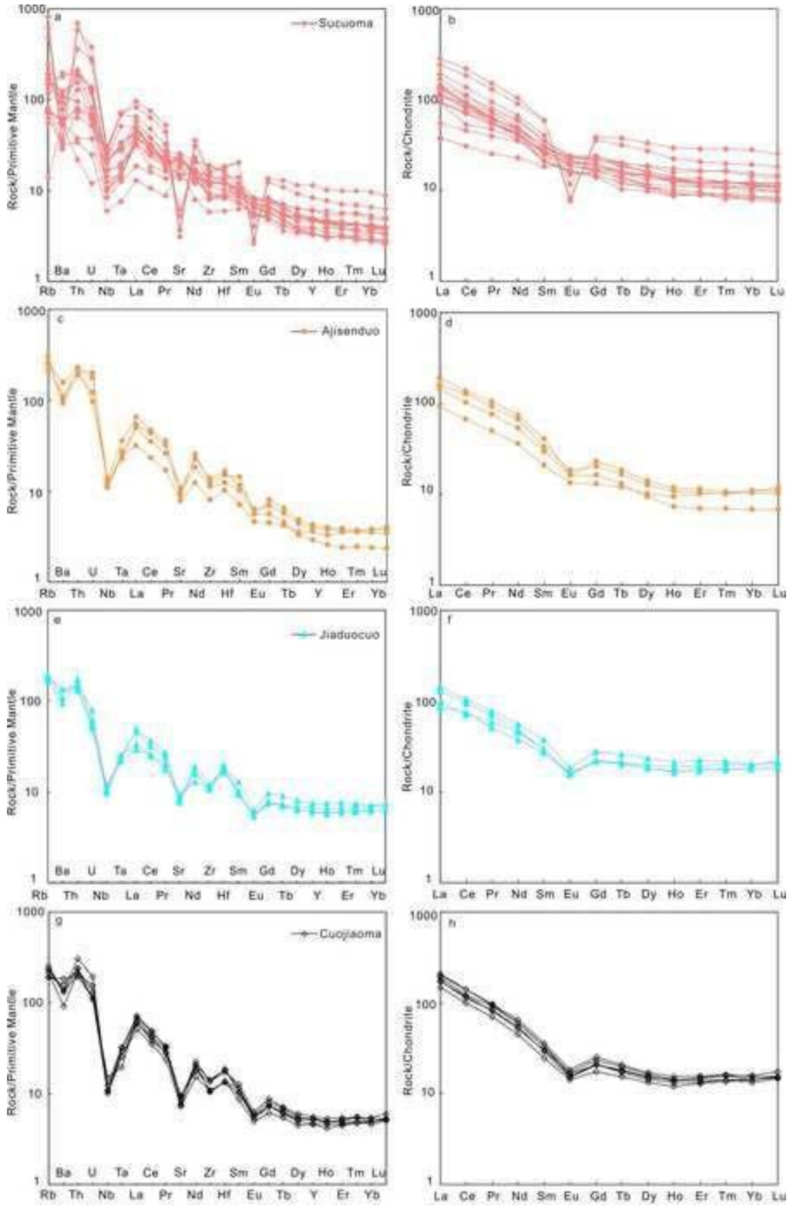

a
Sucuoma
Rock/Primitive Mantle
1000
100
10
1
Rb Ba Th U Nb Ta La Ce Pr Sr Nd Zr Hf Sm Eu Gd Tb Dy Y Ho Er Tm Yb Lu
b
Rock/Chondrite
La Ce Pr Nd Sm Eu Gd Tb Dy Ho Er Tm Yb Lu
c
Ajisenduo
d
e
Jiaduocuo
f
g
Cuojiaoma
h

Fig.8

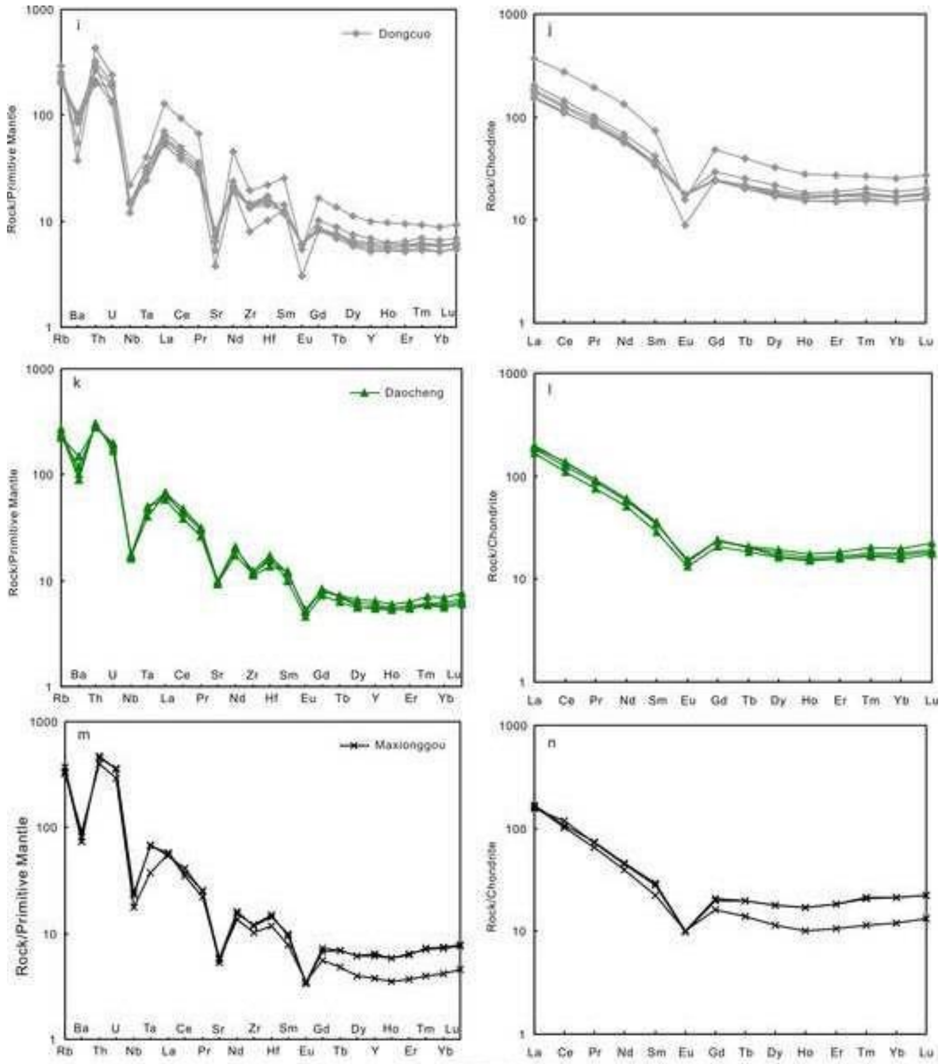

Fig.8 (continued)

870 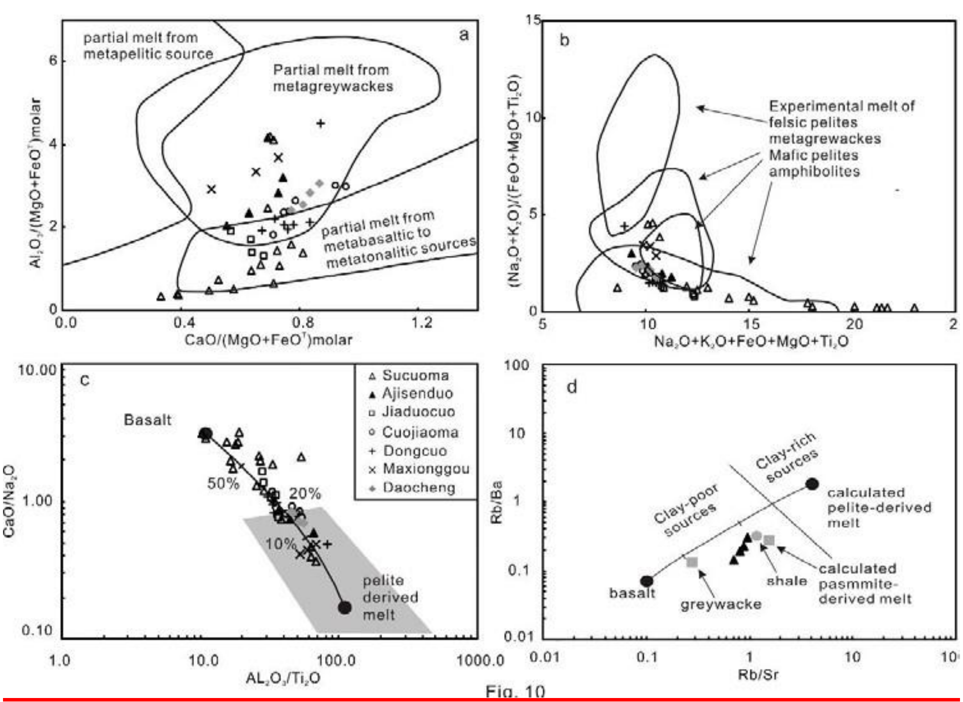
partial melt from metapelitic source
Partial melt from metagreywackes
partial melt from metabasaltic to metatonalitic sources
a
b
Experimental melt of felsic pelites metagrewackes
Mafic pelites amphibolites
c
Basalt
50%
20%
10%
pelite derived melt
Sucuoma
Ajisenduo
Jiaduocuo
Cuojiaoma
Dongcuo
Maxionggou
Daocheng
d
Clay-poor sources
Clay-rich sources
calculated pelite-derived melt
basalt
greywacke
shale
calculated pasmmite-derived melt

Fig. 10

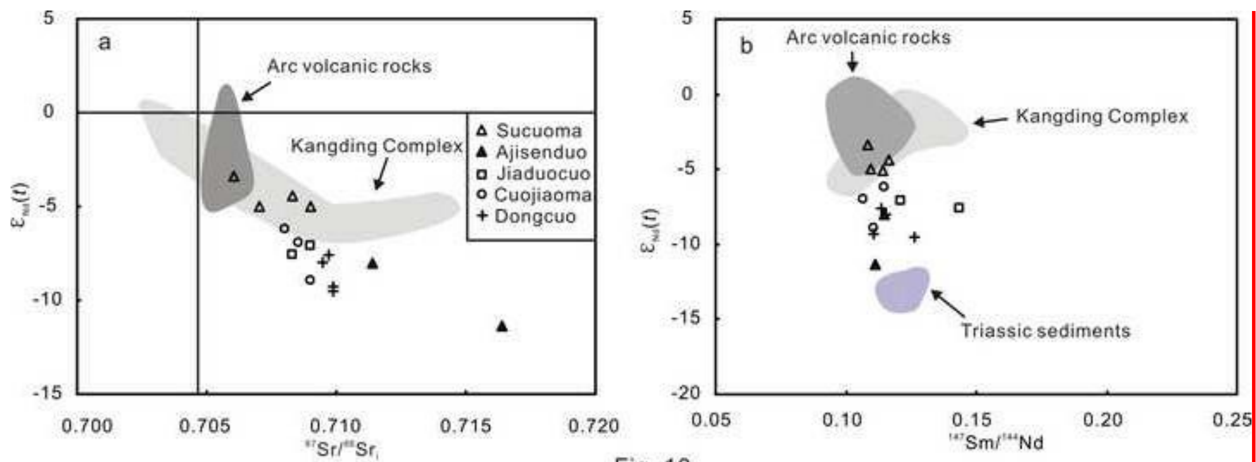
a
Arc volcanic rocks
Kangding Complex
Sucuoma
Ajisenduo
Jiaduocuo
Cuojiaoma
Dongcuo
$\varepsilon_{Nd}(t)$
$^{87}Sr/^{86}Sr_i$
b
Arc volcanic rocks
Kangding Complex
Triassic sediments
$^{147}Sm/^{144}Nd$

Fig. 10

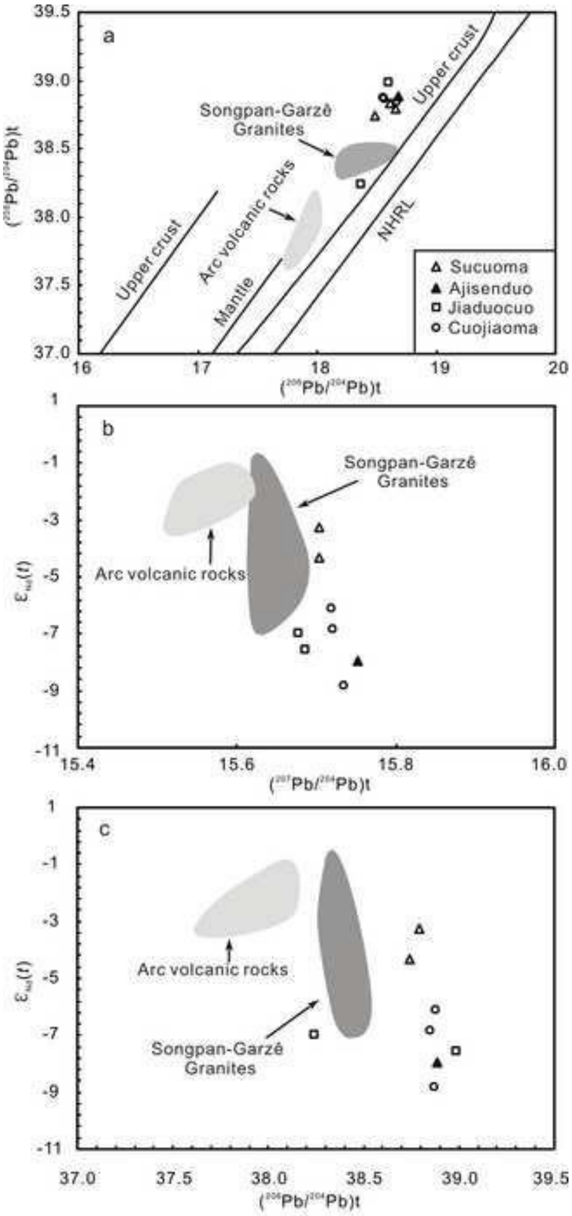

873 Fig. 11

874

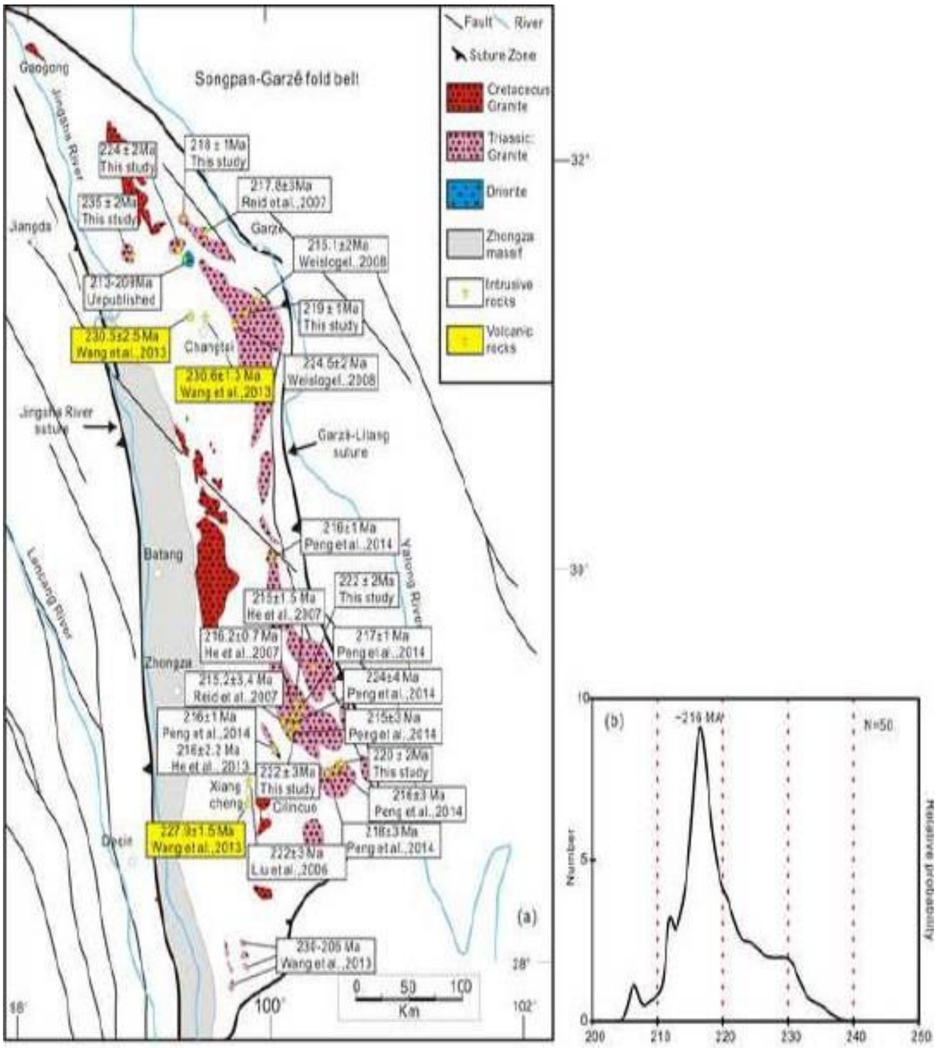
Fault
River
Suture Zone
Cretaceous Granite
Triassic Granite
Diorite
Zhongza massif
Intrusive rocks
Volcanic rocks
Songpan-Garzê fold belt
Jingsha River
Jingsha River suture
Garzê-Litang suture
Yalong River
Lancang River
Batang
Zhongza
Garze
Changtai
Cilincuo
Degin
Xiang cheng
224 ± 2Ma This study
218 ± 1Ma This study
217.6±3Ma Reid et al.,2007
235 ± 2Ma This study
215.1±2Ma Weislogel.,2008
213-209Ma Unpublished
219 ± 1Ma This study
230.5±2.5 Ma Wang et al.,2013
230.6±1.3 Ma Wang et al.,2013
224.5±2 Ma Weislogel.,2008
216±1Ma Peng et al.,2014
222 ± 2Ma This study
217±1 Ma Peng et al.,2014
224±4 Ma Peng et al.,2014
215±3 Ma Peng et al.,2014
220 ± 2Ma This study
216±3 Ma Peng et al.,2014
218±3 Ma Peng et al.,2014
222 ± 3Ma This study
227.9±1.5 Ma Wang et al.,2013
222±3 Ma Liu et al.,2006
234-206 Ma Wang et al.,2013
(a)
0 50 100
Km
100°
102°
28°
30°
32°
(b)
~216 MA
N=50
Number
Relative probability
200
210
220
230
240
250
0
5
10

Fig.12

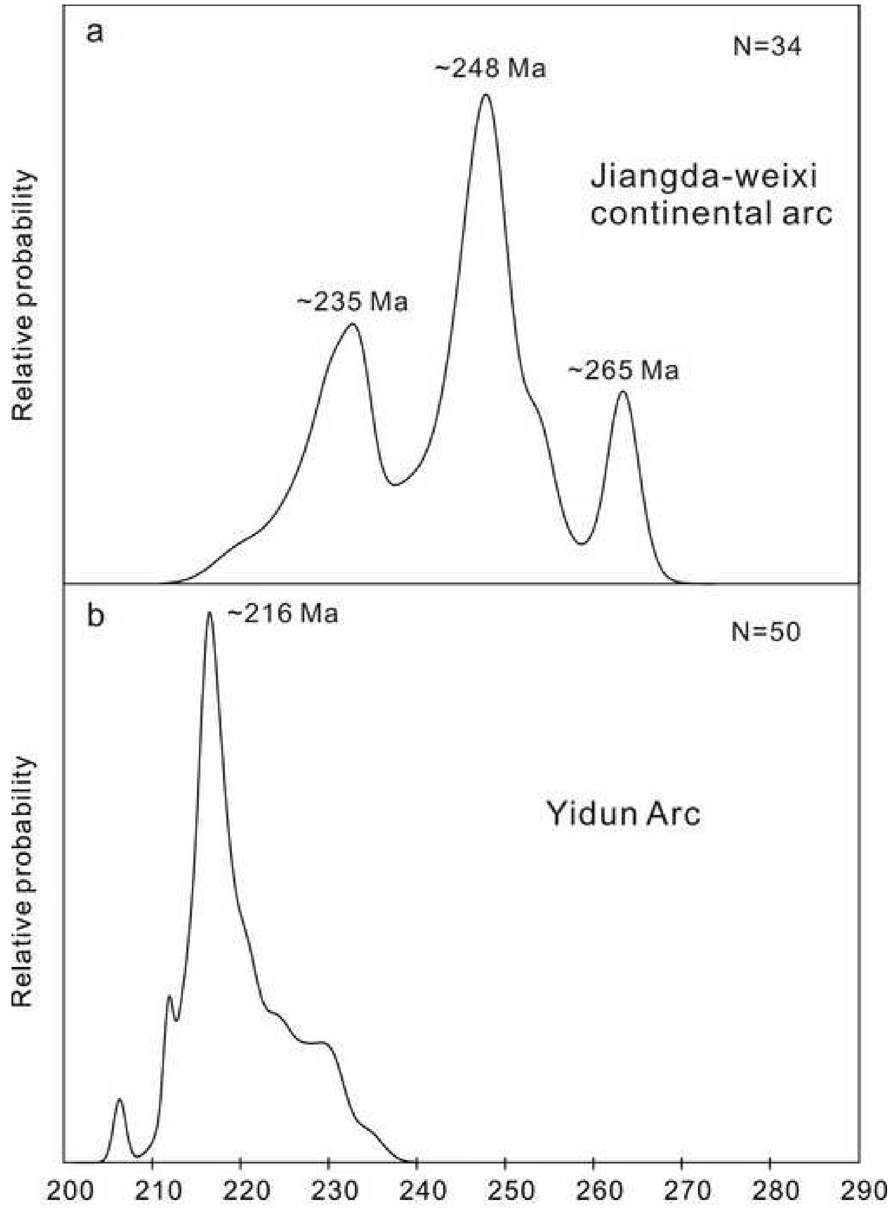
a
N=34
~248 Ma
Jiangda-weixi
continental arc
~235 Ma
~265 Ma
Relative probability
b
~216 Ma
N=50
Yidun Arc
Relative probability
200
210
220
230
240
250
260
270
280
290

Fig. 13

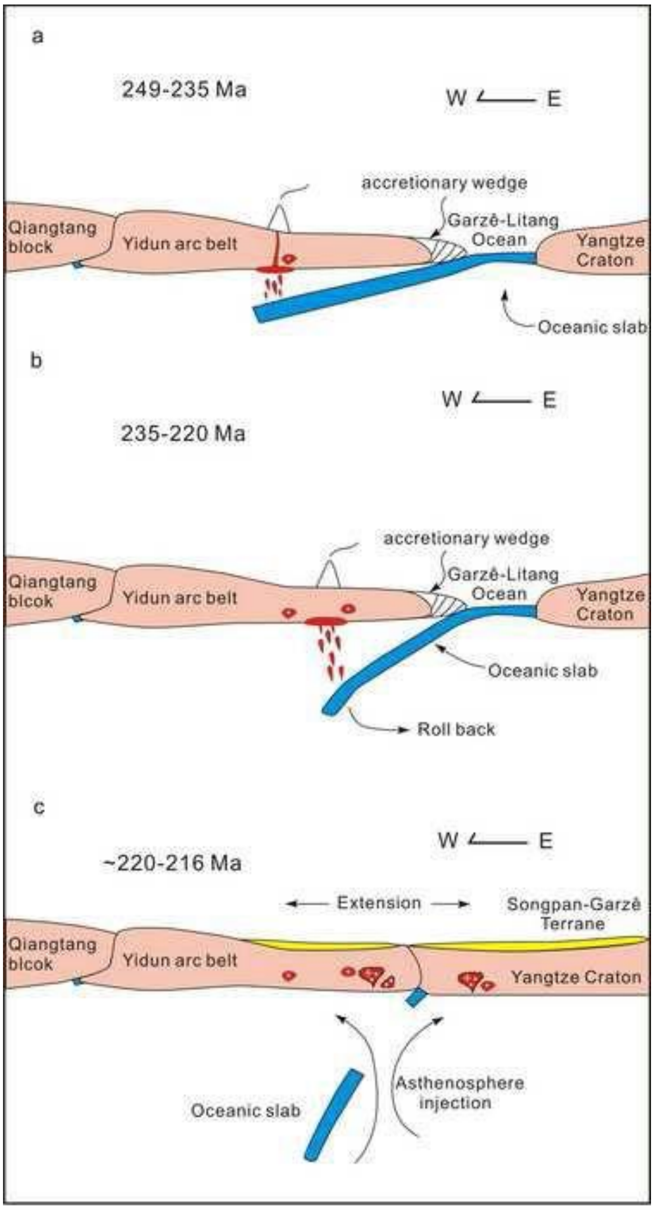
a
249-235 Ma
W E
accretionary wedge
Garzê-Litang
Ocean
Qiangtang
block
Yidun arc belt
Yangtze
Craton
Oceanic slab
b
W E
235-220 Ma
accretionary wedge
Garzê-Litang
Ocean
Qiangtang
blcok
Yidun arc belt
Yangtze
Craton
Oceanic slab
Roll back
c
W E
~220-216 Ma
Extension
Songpan-Garzê
Terrane
Qiangtang
blcok
Yidun arc belt
Yangtze Craton
Asthenosphere
injection
Oceanic slab

879 Fig.14

Table S1 Results of zircon U-Pb LA-ICP-MS analyses of the granitic plutons in the NYAB.

Sample No.	Contents (ppm)			Th/U	$^{207}Pb/^{206}Pb$		$^{207}Pb/^{235}U$		$^{206}Pb/^{238}U$		$^{207}Pb/^{206}Pb$		$^{207}Pb/^{235}U$		$^{206}Pb/^{238}U$	
	Pb	Th	U		Ratio	1σ	Ratio	1σ	Ratio	1σ	Age（Ma）	1σ	Age（Ma）	1σ	Age（Ma）	1σ
Sucuoma pluton																
SCM-10-1	194	1432	4032	0.36	0.06965	0.00207	0.366	0.010	0.03792	0.00043	918	66	317	8	240	3
SCM-10-2	107	959	2434	0.39	0.05103	0.00176	0.258	0.009	0.03639	0.00037	243	80	233	7	230	2
SCM-10-3	125	877	2809	0.31	0.05622	0.00158	0.290	0.008	0.03689	0.00034	461	61	258	7	234	2
SCM-10-4	112	1089	2412	0.45	0.05558	0.00190	0.281	0.009	0.03635	0.00033	435	71	251	7	230	2
SCM-10-5	132	945	2798	0.34	0.06040	0.00170	0.318	0.009	0.03804	0.00048	617	55	280	7	241	3
SCM-10-6	141	1186	3048	0.39	0.05340	0.00141	0.278	0.007	0.03751	0.00038	346	61	249	6	237	2
SCM-10-7	150	1109	3231	0.34	0.05458	0.00140	0.285	0.007	0.03756	0.00029	394	53	254	6	238	2
SCM-10-8	126	1408	2753	0.51	0.05029	0.00133	0.253	0.006	0.03639	0.00034	209	94	229	5	230	2
SCM-10-9	36	369	791	0.47	0.05073	0.00241	0.256	0.012	0.03664	0.00046	228	111	231	10	232	3
SCM-10-10	169	1200	3695	0.32	0.05758	0.00169	0.299	0.009	0.03725	0.00043	522	60	266	7	236	3
SCM-10-11	138	699	3362	0.21	0.04997	0.00158	0.259	0.010	0.03710	0.00080	195	74	234	8	235	5
SCM-10-12	122	1426	2593	0.55	0.04868	0.00136	0.255	0.007	0.03771	0.00040	132	67	230	6	239	2
SCM-10-13	181	1616	4022	0.40	0.05108	0.00117	0.261	0.006	0.03677	0.00034	243	52	236	5	233	2
SCM-10-14	83	815	1837	0.44	0.05126	0.00174	0.259	0.009	0.03652	0.00037	254	78	234	7	231	2
SCM-10-15	171	2091	3488	0.60	0.06525	0.00296	0.342	0.020	0.03690	0.00050	783	96	299	15	234	3
SCM-10-16	183	1516	4102	0.37	0.05312	0.00128	0.272	0.007	0.03677	0.00039	345	54	244	6	233	2
SCM-10-17	181	1338	3991	0.34	0.05391	0.00117	0.282	0.006	0.03772	0.00035	369	50	253	5	239	2
SCM-10-18	131	1271	2814	0.45	0.05225	0.00143	0.270	0.007	0.03728	0.00037	295	68	243	6	236	2
Ajisenduo pluton																
ZK-1-1	97	746	778	0.96	0.05866	0.00204	0.718	0.024	0.08794	0.00098	554	76	550	14	543	6
ZK-1-2	287	2175	6931	0.31	0.05246	0.00134	0.255	0.006	0.03491	0.00033	306	53	231	5	221	2
ZK-1-3	165	241	476	0.51	0.09732	0.00244	3.652	0.090	0.26927	0.00297	1573	47	1561	20	1537	15
ZK-1-4	256	717	4218	0.17	0.05264	0.00149	0.401	0.018	0.05392	0.00186	322	60	342	13	339	11
ZK-1-5	182	847	4500	0.19	0.04943	0.00165	0.249	0.009	0.03614	0.00065	169	84	226	7	229	4
ZK-1-6	146	1018	3455	0.29	0.04886	0.00147	0.242	0.007	0.03578	0.00044	143	66	220	6	227	3
ZK-1-7	156	1259	3655	0.34	0.04944	0.00178	0.246	0.009	0.03574	0.00044	169	83	224	7	226	3
ZK-1-8	172	1257	4130	0.30	0.04740	0.00147	0.233	0.007	0.03533	0.00034	78	65	212	6	224	2
ZK-1-9	220	1743	5227	0.33	0.04974	0.00181	0.247	0.009	0.03582	0.00052	183	85	224	7	227	3
ZK-1-10	322	3244	7396	0.44	0.05302	0.00155	0.258	0.007	0.03488	0.00034	328	67	233	6	221	2
ZK-1-11	150	754	2502	0.30	0.04979	0.00165	0.362	0.013	0.05259	0.00097	183	78	314	10	330	6
ZK-1-12	86	557	2024	0.28	0.04969	0.00174	0.247	0.008	0.03581	0.00034	189	81	224	7	227	2
ZK-1-13	457	3217	10679	0.30	0.05015	0.00152	0.249	0.007	0.03561	0.00055	211	101	226	6	226	3
ZK-1-14	176	1308	3965	0.33	0.06368	0.00199	0.308	0.009	0.03491	0.00044	731	66	273	7	221	3
ZK-1-15	258	1633	6116	0.27	0.05310	0.00140	0.263	0.007	0.03540	0.00040	332	59	237	6	224	2
ZK-1-16	214	1317	5172	0.25	0.05107	0.00162	0.255	0.009	0.03578	0.00048	243	74	231	7	227	3
ZK-1-17	230	1695	5337	0.32	0.05251	0.00137	0.263	0.007	0.03586	0.00036	309	55	237	6	227	2
ZK-1-18	194	1446	1610	0.90	0.05633	0.00187	0.688	0.024	0.08764	0.00107	465	74	532	14	542	6
ZK-1-19	247	1737	5963	0.29	0.05245	0.00122	0.255	0.006	0.03484	0.00032	306	58	230	5	221	2

Jiaduocuo pluton																
JDC-2-1	74	605	1793	0.34	0.05004	0.00160	0.240	0.008	0.03472	0.00038	198	106	219	6	220	2
JDC-2-2	74	816	1771	0.46	0.05225	0.00185	0.248	0.009	0.03448	0.00042	298	81	225	7	219	3
JDC-2-3	71	679	1705	0.40	0.05383	0.00201	0.257	0.009	0.03440	0.00042	365	90	232	8	218	3
JDC-2-4	56	689	1282	0.54	0.05135	0.00207	0.247	0.010	0.03482	0.00044	257	93	224	8	221	3
JDC-2-5	33	387	454	0.85	0.05856	0.00415	0.438	0.033	0.05393	0.00102	550	156	369	23	339	6
JDC-2-6	52	414	1248	0.33	0.05435	0.00345	0.261	0.017	0.03466	0.00073	387	144	235	14	220	5
JDC-2-7	50	577	1169	0.49	0.05166	0.00251	0.244	0.011	0.03454	0.00048	333	118	222	9	219	3
JDC-2-8	63	860	1441	0.60	0.05631	0.00261	0.259	0.011	0.03345	0.00041	465	99	234	9	212	3
JDC-2-9	71	962	1610	0.60	0.05438	0.00225	0.256	0.010	0.03453	0.00049	387	88	231	8	219	3
JDC-2-10	79	764	1855	0.41	0.05383	0.00207	0.253	0.009	0.03425	0.00041	365	90	229	8	217	3
JDC-2-11	56	454	1337	0.34	0.05032	0.00241	0.245	0.013	0.03484	0.00050	209	111	222	10	221	3
JDC-2-12	90	790	2129	0.37	0.05713	0.00260	0.268	0.011	0.03426	0.00046	498	100	241	9	217	3
JDC-2-13	78	687	1883	0.36	0.05266	0.00215	0.251	0.010	0.03466	0.00037	322	93	228	8	220	2
JDC-2-14	102	1169	2418	0.48	0.05087	0.00148	0.243	0.007	0.03446	0.00040	235	69	221	6	218	3
JDC-2-15	66	508	1692	0.30	0.05170	0.00173	0.241	0.008	0.03363	0.00042	272	76	220	7	213	3
JDC-2-16	76	1081	1759	0.61	0.05197	0.00190	0.242	0.009	0.03381	0.00040	283	83	220	7	214	2
JDC-2-17	74	1093	1666	0.66	0.05012	0.00189	0.239	0.009	0.03461	0.00041	211	89	218	7	219	3
JDC-2-18	70	724	1705	0.42	0.05008	0.00177	0.236	0.008	0.03411	0.00043	198	79	215	7	216	3
JDC-2-19	55	716	1286	0.56	0.05174	0.00197	0.248	0.010	0.03447	0.00050	272	92	225	8	218	3
Cuojiaoma pluton																
CJM-6-1	225	952	538	1.77	0.05512	0.00233	0.266	0.016	0.03438	0.00095	417	94	240	13	218	6
CJM-6-2	224	238	596	0.40	0.07075	0.00214	1.049	0.044	0.10729	0.00401	950	62	729	22	657	23
CJM-6-3	65	284	94	3.04	0.04977	0.00382	0.236	0.018	0.03470	0.00088	183	170	215	15	220	5
CJM-6-4	133	586	383	1.53	0.05006	0.00193	0.239	0.010	0.03444	0.00066	198	89	218	8	218	4
CJM-6-5	94	434	211	2.05	0.04937	0.00267	0.238	0.013	0.03480	0.00066	165	126	217	11	221	4
CJM-6-6	84	404	167	2.41	0.05173	0.00327	0.244	0.016	0.03410	0.00070	272	146	222	13	216	4
CJM-6-7	139	623	245	2.54	0.05143	0.00236	0.246	0.011	0.03466	0.00065	261	106	223	9	220	4
CJM-6-8	130	542	217	2.50	0.06051	0.00309	0.291	0.014	0.03500	0.00078	620	109	260	11	222	5
CJM-6-9	192	858	356	2.41	0.05427	0.00267	0.260	0.012	0.03483	0.00074	383	83	235	10	221	5
CJM-6-10	87	320	191	1.68	0.05429	0.00336	0.259	0.015	0.03462	0.00066	383	139	234	12	219	4
CJM-6-11	139	596	384	1.55	0.05399	0.00265	0.259	0.014	0.03446	0.00070	372	109	234	11	218	4
CJM-6-12	135	613	317	1.93	0.05185	0.00217	0.247	0.010	0.03433	0.00057	280	92	224	8	218	4
CJM-6-13	97	460	170	2.71	0.05163	0.00354	0.251	0.017	0.03530	0.00095	333	157	228	14	224	6
CJM-6-14	182	811	394	2.06	0.05456	0.00219	0.261	0.011	0.03464	0.00071	394	91	236	9	220	4
CJM-6-15	89	430	136	3.16	0.05060	0.00378	0.245	0.019	0.03505	0.00083	233	174	223	15	222	5
CJM-6-16	186	889	375	2.37	0.05356	0.00238	0.255	0.011	0.03437	0.00061	354	97	230	9	218	4
Dongcuo pluton																
HZS-8-1	696	893	1315	0.68	0.05461	0.00228	0.264	0.011	0.03501	0.00040	398	94	238	9	222	2
HZS-8-2	2167	3001	4842	0.62	0.05352	0.00109	0.259	0.006	0.03504	0.00031	350	44	234	5	222	2
HZS-8-3	1693	477	1020	0.47	0.05515	0.00367	0.265	0.018	0.03482	0.00046	417	150	239	15	221	3
HZS-8-4	1256	803	1781	0.45	0.05202	0.00225	0.251	0.011	0.03542	0.00056	287	100	228	9	224	3
HZS-8-5	3097	1606	3730	0.43	0.06159	0.00136	0.294	0.006	0.03497	0.00040	661	46	262	5	222	3
HZS-8-6	966	782	2037	0.38	0.05507	0.00215	0.267	0.011	0.03516	0.00045	417	87	241	8	223	3

HZS-8-7	1189	774	1782	0.43	0.05629	0.00167	0.274	0.008	0.03523	0.00037	465	65	246	6	223	2
HZS-8-8	2150	1072	2238	0.48	0.05638	0.00202	0.266	0.008	0.03466	0.00061	478	80	239	7	220	4
HZS-8-9	2593	561	1474	0.38	0.04835	0.00189	0.236	0.009	0.03516	0.00046	117	93	215	8	223	3
HZS-8-10	1952	1075	2427	0.44	0.05267	0.00290	0.260	0.014	0.03551	0.00040	322	126	234	11	225	3
HZS-8-11	2017	438	827	0.53	0.11183	0.00234	4.837	0.100	0.31201	0.00298	1829	71	1791	17	1751	15
HZS-8-12	1594	950	2111	0.45	0.05254	0.00189	0.256	0.009	0.03535	0.00040	309	77	231	7	224	2
HZS-8-13	2373	1160	1986	0.58	0.06228	0.00217	0.297	0.011	0.03431	0.00040	683	79	264	8	217	2
HZS-14-1	309	818	1447	0.57	0.07676	0.00169	1.832	0.044	0.17163	0.00195	1117	43	1057	16	1021	11
HZS-14-2	40	410	956	0.43	0.05631	0.00296	0.273	0.014	0.03536	0.00049	465	117	245	11	224	3
HZS-14-3	74	623	1829	0.34	0.05361	0.00218	0.260	0.010	0.03527	0.00047	354	91	234	8	223	3
HZS-14-4	60	466	1455	0.32	0.05088	0.00224	0.252	0.011	0.03590	0.00053	235	106	228	9	227	3
HZS-14-5	93	669	2258	0.30	0.05258	0.00172	0.258	0.008	0.03547	0.00034	309	74	233	7	225	2
HZS-14-6	64	469	1542	0.30	0.05812	0.00255	0.290	0.014	0.03600	0.00052	600	96	258	11	228	3
HZS-14-7	64	782	1491	0.52	0.05353	0.00306	0.257	0.015	0.03479	0.00047	350	130	232	12	220	3
HZS-14-8	72	186	1153	0.16	0.05802	0.00197	0.434	0.015	0.05437	0.00088	532	79	366	11	341	5
HZS-14-9	70	275	422	0.65	0.06620	0.00225	1.196	0.041	0.13059	0.00161	813	72	799	19	791	9
HZS-14-10	107	194	815	0.24	0.05901	0.00171	0.940	0.027	0.11520	0.00139	569	63	673	14	703	8
HZS-14-11	84	733	2054	0.36	0.05215	0.00180	0.250	0.008	0.03484	0.00037	300	80	226	7	221	2
HZS-14-12	509	387	1234	0.31	0.12795	0.00213	6.074	0.124	0.34230	0.00472	2070	29	1987	18	1898	23
HZS-14-13	68	758	1632	0.46	0.05279	0.00178	0.248	0.008	0.03423	0.00043	320	76	225	7	217	3
HZS-14-14	27	275	641	0.43	0.05619	0.00406	0.262	0.018	0.03415	0.00048	461	156	236	15	216	3
Daocheng pluton																
DC-9-1	114	1320	2628	0.50	0.05424	0.00230	0.261	0.010	0.03511	0.00073	389	94	236	8	222	5
DC-9-2	109	968	2552	0.38	0.05260	0.00202	0.258	0.009	0.03556	0.00049	322	89	233	8	225	3
DC-9-3	154	2179	3476	0.63	0.05173	0.00155	0.245	0.007	0.03415	0.00035	272	66	222	6	216	2
DC-9-4	121	1069	2907	0.37	0.05121	0.00139	0.240	0.007	0.03366	0.00031	250	68	218	5	213	2
DC-9-5	102	843	2395	0.35	0.05097	0.00168	0.245	0.008	0.03454	0.00034	239	81	223	7	219	2
DC-9-6	134	1195	3139	0.38	0.05091	0.00121	0.247	0.006	0.03487	0.00033	235	56	225	5	221	2
DC-9-7	110	849	2580	0.33	0.05285	0.00196	0.262	0.011	0.03555	0.00049	324	85	236	9	225	3
DC-9-8	79	743	1894	0.39	0.05041	0.00190	0.239	0.009	0.03431	0.00039	213	87	218	7	217	2
DC-9-9	128	1152	3084	0.37	0.05069	0.00163	0.246	0.008	0.03481	0.00040	233	74	223	7	221	2
DC-9-10	55	645	1288	0.50	0.04933	0.00260	0.242	0.013	0.03515	0.00053	165	124	220	11	223	3
DC-9-11	89	766	2158	0.35	0.04896	0.00245	0.239	0.012	0.03536	0.00059	146	112	218	10	224	4
DC-9-12	162	1418	3846	0.37	0.05478	0.00167	0.270	0.009	0.03544	0.00039	467	67	243	7	225	2
DC-9-13	88	1133	1970	0.58	0.05071	0.00249	0.248	0.012	0.03555	0.00058	228	118	225	10	225	4
DC-9-14	115	1187	2674	0.44	0.04609	0.00148	0.225	0.007	0.03542	0.00038	400	(320)	206	6	224	2
DC-9-15	92	971	2151	0.45	0.05050	0.00171	0.248	0.009	0.03534	0.00058	217	47	225	7	224	4
DC-9-16	141	1748	3291	0.53	0.04874	0.00160	0.232	0.007	0.03451	0.00044	200	76	212	6	219	3
Maxionggou pluton																
MXG-1-1	316	1457	3160	0.46	0.05574	0.00193	0.277	0.011	0.03574	0.00053	443	78	248	8	226	3
MXG-1-2	1133	6276	10091	0.62	0.05116	0.00107	0.257	0.005	0.03615	0.00029	256	48	233	4	229	2
MXG-1-3	530	2492	4919	0.51	0.05745	0.00214	0.280	0.011	0.03500	0.00040	509	78	251	9	222	2
MXG-1-4	988	5610	8102	0.69	0.05102	0.00129	0.247	0.006	0.03482	0.00035	243	57	224	5	221	2

MXG-1-5	341	1646	3982	0.41	0.05364	0.00147	0.261	0.007	0.03511	0.00037	367	58	236	6	222	2
MXG-1-6	576	2610	5171	0.50	0.05953	0.00151	0.294	0.007	0.03566	0.00039	587	54	261	5	226	2
MXG-1-7	373	1970	3298	0.60	0.05222	0.00179	0.254	0.008	0.03512	0.00036	295	80	230	7	222	2
MXG-1-8	473	2136	4852	0.44	0.05516	0.00140	0.268	0.007	0.03490	0.00046	420	57	241	6	221	3
MXG-1-9	725	3123	9677	0.32	0.04973	0.00116	0.251	0.006	0.03620	0.00037	189	54	228	5	229	2
MXG-1-10	880	3633	8748	0.42	0.05815	0.00141	0.289	0.007	0.03565	0.00036	600	54	258	5	226	2
MXG-1-11	623	2998	6332	0.47	0.05497	0.00116	0.269	0.006	0.03512	0.00033	409	48	242	5	223	2
MXG-1-12	634	1930	8428	0.23	0.05707	0.00113	0.284	0.006	0.03578	0.00034	494	44	254	5	227	2
MXG-1-13	971	4502	8733	0.52	0.06158	0.00092	0.308	0.005	0.03604	0.00025	661	36	272	4	228	2
MXG-1-14	495	2431	5735	0.42	0.05188	0.00102	0.254	0.005	0.03525	0.00019	280	44	230	4	223	1
MXG-1-15	934	4103	10871	0.38	0.05291	0.00093	0.292	0.005	0.03977	0.00038	324	41	260	4	251	2
MXG-1-16	558	2181	6563	0.33	0.06237	0.00192	0.313	0.010	0.03612	0.00036	687	65	276	7	229	2

Formatted: Line spacing: Exactly 10 pt, Don't allow hanging punctuation

Table S2 Zircon Hf isotopic data of samples from the Ajisenduo (ZK-1), Sucuoma (SCM-10), Jiaduocuo (JDC-2) and Dongcuo (HZS-8) plutons

Sample	Age(Ma)	$^{176}Hf/^{177}Hf$	2σ	$^{176}Lu/^{177}Hf$	2σ	$^{176}Yb/^{177}Hf$	2σ	εHf(t)	2σ	T_{DM1}	2σ	T_{DM2}	2σ	fLu/Hf
Ajisenduo pluton														
ZK-1-1	224	0.282407	0.000023	0.001332	0.000017	0.036351	0.000607	-8.2	0.81	1206	65	1773	102	-0.96
ZK-1-2	224	0.282424	0.000016	0.001558	0.000055	0.042806	0.001454	-7.6	0.57	1188	46	1736	72	-0.95
ZK-1-3	224	0.282393	0.000017	0.001556	0.000071	0.044277	0.002120	-8.7	0.59	1233	47	1806	74	-0.95
ZK-1-4	224	0.282434	0.000016	0.001256	0.000062	0.034429	0.001936	-7.2	0.56	1165	45	1711	71	-0.96
ZK-1-5	224	0.282454	0.000017	0.003215	0.000095	0.092053	0.001912	-6.8	0.59	1200	49	1685	74	-0.90
ZK-1-6	224	0.282300	0.000017	0.001021	0.000055	0.030513	0.001995	-11.9	0.60	1346	48	2008	76	-0.97
ZK-1-7	224	0.282503	0.000019	0.001490	0.000053	0.040681	0.001901	-4.8	0.68	1075	55	1561	86	-0.96
ZK-1-8	224	0.282419	0.000017	0.001559	0.000032	0.045189	0.000589	-7.8	0.61	1195	49	1747	77	-0.95
ZK-1-9	224	0.282436	0.000019	0.001487	0.000061	0.044182	0.001908	-7.2	0.68	1170	55	1709	86	-0.96
ZK-1-10	224	0.282420	0.000019	0.001683	0.000020	0.049462	0.000446	-7.8	0.66	1199	53	1748	83	-0.95
ZK-1-11	224	0.282484	0.000020	0.001266	0.000048	0.036655	0.001387	-5.5	0.71	1095	57	1600	90	-0.96
ZK-1-12	224	0.282454	0.000028	0.001472	0.000121	0.044826	0.004091	-6.6	0.99	1144	80	1669	125	-0.96
Sucuoma pluton														
SCM-10-1	235	0.282610	0.000020	0.000920	0.000014	0.025271	0.000278	-0.7	0.69	907	55	1307	88	-0.97
SCM-10-2	235	0.282609	0.000020	0.000929	0.000050	0.024217	0.001415	-0.7	0.70	909	56	1310	89	-0.97
SCM-10-3	235	0.282606	0.000019	0.001260	0.000052	0.033789	0.001510	-0.9	0.69	922	55	1320	87	-0.96
SCM-10-4	235	0.282628	0.000022	0.001013	0.000033	0.027112	0.000603	-0.1	0.78	885	62	1270	98	-0.97
SCM-10-5	235	0.282589	0.000020	0.001095	0.000022	0.029362	0.000465	-1.5	0.71	941	56	1356	89	-0.97
SCM-10-6	235	0.282598	0.000016	0.001209	0.000029	0.032479	0.000666	-1.2	0.58	932	47	1337	74	-0.96
SCM-10-7	235	0.282611	0.000026	0.000857	0.000050	0.021675	0.001170	-0.7	0.90	905	72	1305	114	-0.97
SCM-10-8	235	0.282613	0.000020	0.000774	0.000027	0.020100	0.000665	-0.6	0.72	900	57	1300	91	-0.98
SCM-10-9	235	0.282608	0.000019	0.001309	0.000033	0.035460	0.001088	-0.8	0.68	920	55	1316	87	-0.96
SCM-10-10	235	0.282585	0.000019	0.000981	0.000019	0.026235	0.000387	-1.6	0.67	945	53	1365	84	-0.97
SCM-10-11	235	0.282608	0.000016	0.001085	0.000011	0.029495	0.000380	-0.8	0.57	915	46	1314	73	-0.97
SCM-10-12	235	0.282608	0.000024	0.001212	0.000053	0.032500	0.001706	-0.8	0.84	918	67	1316	106	-0.96
SCM-10-13	235	0.282619	0.000019	0.001192	0.000058	0.031282	0.001467	-0.4	0.68	901	54	1290	86	-0.96
Jiaduocuo pluton														
JDC-2-1	218	0.282599	0.000018	0.001723	0.000071	0.051179	0.002348	-1.6	0.62	944	51	1350	79	-0.95
JDC-2-2	218	0.282576	0.000018	0.001314	0.000067	0.038465	0.001701	-2.4	0.64	966	52	1399	82	-0.96
JDC-2-3	218	0.282587	0.000022	0.001287	0.000023	0.036772	0.000592	-2.0	0.76	950	61	1374	97	-0.96
JDC-2-4	218	0.282584	0.000022	0.001232	0.000050	0.035200	0.001131	-2.0	0.77	953	61	1380	97	-0.96
JDC-2-5	218	0.282612	0.000021	0.001230	0.000018	0.034698	0.000252	-1.0	0.73	912	58	1316	92	-0.96
JDC-2-6	218	0.282591	0.000017	0.001071	0.000003	0.032554	0.000433	-1.8	0.60	938	48	1362	77	-0.97
JDC-2-7	218	0.282574	0.000018	0.001552	0.000119	0.045757	0.004141	-2.4	0.62	974	50	1404	79	-0.95
JDC-2-8	218	0.282650	0.000018	0.001694	0.000026	0.052171	0.000557	0.2	0.64	870	52	1236	82	-0.95
JDC-2-9	218	0.282562	0.000026	0.002442	0.000047	0.069490	0.001211	-3.0	0.93	1017	77	1440	118	-0.93
JDC-2-10	218	0.282619	0.000019	0.001072	0.000060	0.030566	0.001887	-0.8	0.68	899	55	1300	87	-0.97
JDC-2-11	218	0.282613	0.000023	0.001489	0.000052	0.045945	0.001357	-1.0	0.83	917	67	1316	105	-0.96
JDC-2-12	218	0.282551	0.000027	0.001481	0.000057	0.046613	0.001666	-3.2	0.94	1005	76	1454	119	-0.96
JDC-2-13	218	0.282614	0.000021	0.001047	0.000003	0.032774	0.000397	-0.9	0.75	905	60	1309	95	-0.97
Duocuo pluton														

HZS-8-1	222	0.282518	0.000017	0.000977	0.000014	0.028789	0.000661	-4.3	0.62	1038	49	1522	78	-0.97
HZS-8-2	222	0.282463	0.000023	0.001615	0.000097	0.050345	0.003103	-6.3	0.83	1135	67	1650	105	-0.95
HZS-8-3	222	0.282527	0.000015	0.001504	0.000056	0.045565	0.001413	-4.0	0.54	1040	44	1507	68	-0.95
HZS-8-4	222	0.282409	0.000019	0.001638	0.000038	0.044144	0.000647	-8.2	0.66	1213	53	1772	83	-0.95
HZS-8-5	222	0.282600	0.000020	0.001584	0.000023	0.046821	0.001108	-1.4	0.71	938	57	1344	90	-0.95
HZS-8-6	222	0.282538	0.000016	0.001158	0.000039	0.033938	0.001432	-3.6	0.56	1015	45	1479	71	-0.97
HZS-8-7	222	0.282522	0.000018	0.000926	0.000017	0.026628	0.000354	-4.1	0.64	1032	51	1514	82	-0.97
HZS-8-8	222	0.282513	0.000019	0.001071	0.000038	0.031749	0.001217	-4.5	0.68	1049	54	1535	86	-0.97
HZS-8-9	222	0.282531	0.000018	0.001128	0.000054	0.033557	0.001587	-3.8	0.64	1024	51	1494	81	-0.97
HZS-8-10	222	0.282507	0.000015	0.001259	0.000012	0.037316	0.000204	-4.7	0.54	1063	43	1551	68	-0.96
HZS-8-11	222	0.282595	0.000018	0.000816	0.000012	0.023902	0.000532	-1.5	0.62	927	49	1349	79	-0.98
HZS-8-12	222	0.282550	0.000015	0.001261	0.000021	0.037086	0.000738	-3.2	0.53	1001	42	1453	67	-0.96
HZS-8-13	222	0.282521	0.000013	0.000892	0.000018	0.025350	0.000374	-4.2	0.47	1033	38	1516	60	-0.97

Table S4 The published geochronological data of Jiangda-Weixi belt

Intrusion/ Vol.	Lithology	Methodology	Age	Source
Gongka	Granodiorite	La-ICP-MS	232 ± 5 Ma	Gao et al., 2010
Yangla	Granodiorite	La-ICP-MS	230 ± 4 Ma	
Yangla	Monzonite	La-ICP-MS	261 ± 3 Ma	
Tongpu	Granite	La-ICP-MS	264 ± 2 Ma	Wu et al., 2013
Tongpu	Quartz diorite	La-ICP-MS	263 ± 2 Ma	
Tongpu	Granodiorite	La-ICP-MS	264 ± 2 Ma	
Deqin	Granodiorite	La-ICP-MS	255 ± 2 Ma	Zhang et al., 2011
Deqin	diorite	La-ICP-MS	254 ± 2 Ma	
Baimaxueshan	diorite	SHRIMP	251 ± 2 Ma	Zi et al., 2012a
Baimaxueshan	tonalite	SHRIMP	253 ± 4 Ma	
Baimaxueshan	Granodiorite	SHRIMP	249 ± 2 Ma	
Baimaxueshan	Granodiorite	SHRIMP	248 ± 2 Ma	
Renzhixueshan	Rhyolite	La-ICP-MS	247 ± 2 Ma	Wang et al., 2011
Renzhixueshan	Rhyolite	La-ICP-MS	249 ± 2 Ma	
Pantiange	Rhyolite	SHRIMP	247 ± 3 Ma	Zi et al., 2012b
Pantiange	Rhyolite	SHRIMP	246 ± 3 Ma	
Low Cuiyibi	Basalt	SHRIMP	245 ± 4 Ma	
Upper Cuiyibi	Basalt	SHRIMP	237 ± 3 Ma	
Low Cuiyibi	Rhyolite	SHRIMP	242 ± 3 Ma	
Upper Cuiyibi	Rhyodacite	SHRIMP	239 ± 3 Ma	
Ludian	Monzogranite	SHRIMP	228 ± 3 Ma	Zi et al.,2013
Ludian	Granodiorite	SHRIMP	226 ± 3 Ma	
Ludian	Monzogranite	SHRIMP	220 ± 3 Ma	
Ludian	Monzogranite	SHRIMP	231 ± 3 Ma	
Ludian	Granodiorite	SHRIMP	230 ± 2 Ma	
Beiwu	Granodiorite	SIMS	234 ± 1 Ma	Zhu et al., 2011
Linong	Granite	SIMS	233 ± 2 Ma	
Lunong	Granodiorite	SIMS	231 ± 2 Ma	
Renzhixueshan–Pantiange	Rhyolite	La-ICP-MS	245 ± 3 Ma	Wang et al., 2013
Renzhixueshan–Pantiange	Rhyolite	La-ICP-MS	247 ± 3 Ma	
Renzhixueshan–Pantiange	Rhyolite	La-ICP-MS	246 ± 2 Ma	
Renzhixueshan–Pantiange	Rhyolite	La-ICP-MS	248 ± 2 Ma	
Renzhixueshan–Pantiange	Rhyolite	La-ICP-MS	249 ± 2 Ma	
Renzhixueshan–Pantiange	Basalt	La-ICP-MS	246 ± 2 Ma	

Formatted : Font color: Auto

Formatted: Body Text, Line spacing: single, Don't allow hanging punctuation